Lehigh University
Lehigh Preserve

Theses and Dissertations

1992

Thermal management of second level electronic packages

Masdi Muhammad
Lehigh University

Follow this and additional works at: http://preserve.lehigh.edu/etd

Recommended Citation
Muhammad, Masdi, "Thermal management of second level electronic packages" (1992). *Theses and Dissertations.* Paper 84.

This Thesis is brought to you for free and open access by Lehigh Preserve. It has been accepted for inclusion in Theses and Dissertations by an authorized administrator of Lehigh Preserve. For more information, please contact preserve@lehigh.edu.

AUTHOR: Muhammad, Masdi

TITLE:

Thermal Management of Second Level Electronic Packages

DATE: MAY 31, 1992

Thermal Management of Second Level Electronic Packages

BY

Masdi Muhammad

A THESIS
PRESENTED TO THE GRADUATE COMMITTEE
OF LEHIGH UNIVERSITY
IN CANDIDACY FOR THE DEGREE OF
MASTER OF SCIENCE IN
MANUFACTURING SYSTEMS ENGINEERING

LEHIGH UNIVERSITY
BETHLEHEM, PENNSYLVANIA
1992

This thesis is accepted and approved in partial fulfillment of the requirement for the degree of Master of Science in Manufacturing System Engineering.

May 12, 1992

Date

_____

Advisor in Charge

_____

Chairman, Mechanical Engineering
and Mechanics

This thesis is dedicated to
my lovely wife, Lily,
and
my firstborn, M. Kushairy

ACKNOWLEDGEMENTS

I am pleased to thank the many talented people who have helped me in one way or another to the successful completion of this thesis. Particular thanks are due to my dearest advisor, Dr. Antonios Liakopoulos for his unending support and encouragement. His wealth of knowledge and experience in the field has given me more insights and understanding on the subject of this thesis. My many thanks also go to a good friend, Xiaobo Huang for his help in this study. I am indebted to the Center for Manufacturing Systems Engineering and Lehigh University for granting me the research assistantship and for making this study possible.

I would also like to thank my wife and my parents for their continuing love and support throughout the entire years of my study.

Lastly, many thanks to all my friends especially Nizam, Liza and Iskandar for making my life here at Lehigh a good and memorable one.

TABLE OF CONTENTS

LIST OF FIGURES

NOMENCLATURE

A	Cavity aspect ratio
Co	Courant number
E	Activation energy
F_t	Temperature related failure rate
g	Acceleration due to gravity
Gr	Grashof number
Gr_c	Critical Grashof number
h_c	Protrusion width
h	Total cavity height
j	Unit vector in y direction
k	Thermal conductivity
k_1	Boltzman constant
l_c	Heating element length
l_s	Heating element spacing
l	Cavity width
Nu	Nusselt number
p	Pressure
Pr	Prandtl number
q"	Applied heat flux

q_L	Heat transfer rate from left wall
q_R	Heat transfer rate from right wall
R_{JT0}	Rate of failure at reference temperature
R_{JT1}	Rate of failure at T_1
Ra	Rayleigh number
t	Time
T	Temperature
x,y	Cartesian coordinates
$\underline{v}$=(u,v)	Velocity vector

Greek Symbols

α	Thermal diffusivity
β	Coefficient of thermal expansion
ν	Kinematic viscosity
ρ	Density
ψ	Streamfunction

Note : '*' denotes non-dimensional variables

ABSTRACT

The mean time between failures (MTBF) of electronic equipment depends strongly on the temperature in which the equipment operates. One way to increase the reliability is to reduce the operating temperature and keep it within specified reliability limits. This calls for effective thermal management especially in electronic equipment characterized by compact microchip design. Many approaches are used in reducing the operating temperature ranging from natural convection with air as the medium to sophisticated conduction cooling. Product price and performance requirements dictate the choice of cooling mode.

The present study deals with the cooling of electronic equipment using natural convection with air as the medium. A mathematical model describing the thermal and flow phenomena encountered in cooling typical second level electronic packages has been developed. The governing equations are solved numerically and the temperature fields are calculated for Grashof number values ranging from zero (conduction) to 1.5×10^6. Both laminar and turbulent flows have been studied for two different geometry cases. The Grashof number is based on cavity width.

The results indicate that the maximum non-dimensional temperature decreases as the Grashof number increases for both geometries. At high values of

Grashof number the air flow looses its stability and becomes oscillatory in time which in turn enhances the rates of heat transfer.

In view of the complexity of the problem, further analysis is required including the determination of resonant configurations that can either maximize the heat transfer or at least avoid the adverse conditions leading to local hot spots. Information from these studies should be used in planning complex architectures that arise in electronic devices.

CHAPTER ONE

INTRODUCTION

Present efforts to produce faster and more powerful microelectronic devices have an enormous impact on the thermal management of electronic components and systems. Microchips that have densely packed gates require high power consumption. This increases the power density and thereby generates large heat fluxes. The increase in heat flux leads to increased operating temperature and ultimately reduces the reliability of the component. The density at which the chips are packed on printed circuit boards (PCB) is so high that heat removal has become a major problem. About 40 percent of all failures in electronic equipment is caused by temperature, either too high or too low or the cycling temperature effects [Fuqua, 1987]. Generally, the optimum working temperature for electronic equipment is room temperature but in practice, it is impossible to keep the temperature constant since operation generates heat. The heat generated has to be removed in order to keep the temperature rise minimal and therefore to increase the reliability significantly.

Keeping the operating temperatures of electronic components relatively constant within the specified reliability limits is the primary method for improving reliability. Cooling techniques for electronic equipment range from free convection, using air as the medium, to sophisticated liquid cooling approaches. Choosing the most

efficient cooling method is important since inadequate thermal management can reduce reliability whereas excessive cooling can dramatically increase manufacturing and operating costs. Free convection has been the most widely used technique in cooling moderately heated equipment, such as the low cost dot matrix printers, personal computers and workstations, because it is the simplest, most economical and reliable method. Besides, interference with sensitive electronic component is eliminated by using natural convection. The natural or free convection cooling is created by the existence of temperature gradients. This temperature gradient causes changes in air density and consequently the cold or denser air moves down replacing the hotter air that is moving up. This circulatory motion of air improves the cooling rate. The efficiency of natural convection can be maximized by properly choosing the air paths. For higher product price and performance, e.g. the Cray supercomputers, conduction cooling is preferred in order to maintain the very low junction temperature required for extremely high reliability [Dally, 1990].

Electronic packaging can be defined as the placement and connection of many electronic components in an enclosure to protect the system from environmental damage and simultaneously provide easy access for routine maintenance. There are several levels of electronic packaging involved in an electronic system. Referring to Figure 1.1, the packaging of electronic components starts from the housing of a fragile chip which has been fabricated on silicon wafer. The housing which is called carrier

(first level packaging), provides all the necessary wiring as an interface between the chip and the printed circuit board. The carrier is mounted onto a PCB (second level packaging) and placed in back panel where communication among several PCBs is possible.

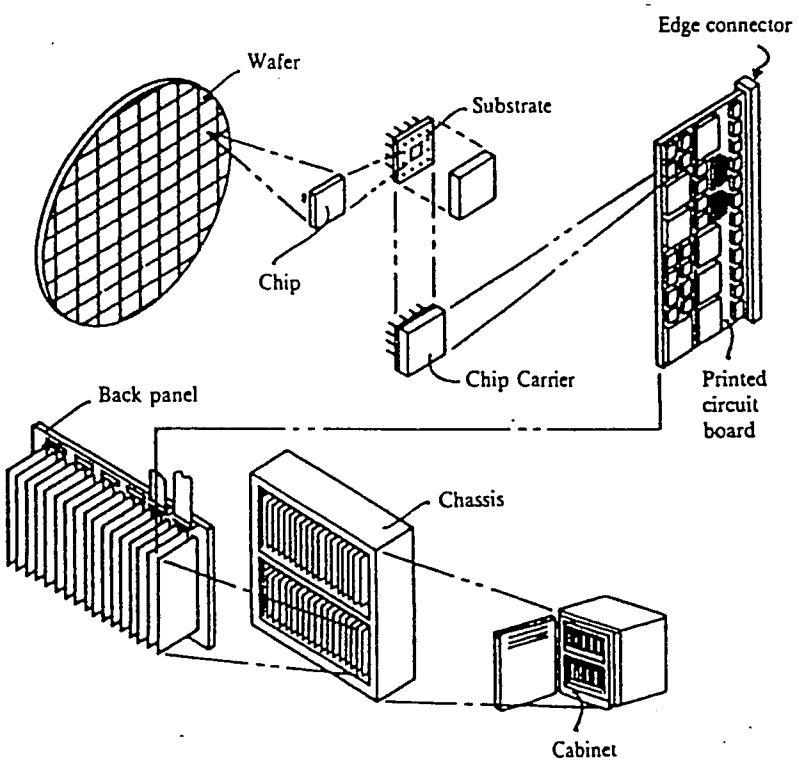

Figure 1.1
Levels of electronic packaging, [Dally, 1990]

1.1 Levels of Packaging in Electronic Equipment

There are several levels of packaging in electronic equipment as shown in Figure 1.1. The present study deals primarily with second level packaging. However, it is helpful to discuss briefly some aspects of the first level packaging.

First level package (chip carrier) is the housing of thin and fragile silicon chip. One example is the plastic dual-in-line package (DIP). This packaging is important not only to protect the chip from physical damage but also to serve as interconnection to the circuit boards. In operation, chip carriers are also involved in the heat transfer process. The heat generated by the chip has to pass through the chip carrier first before it can be removed. The schematic of a typical chip carrier is shown in Figure 1.2 [Dally, 1990]. Even though this type of chip carrier is commonly used, it can severely limit the heat transfer process because of the thermal insulators used at the top and bottom surfaces.

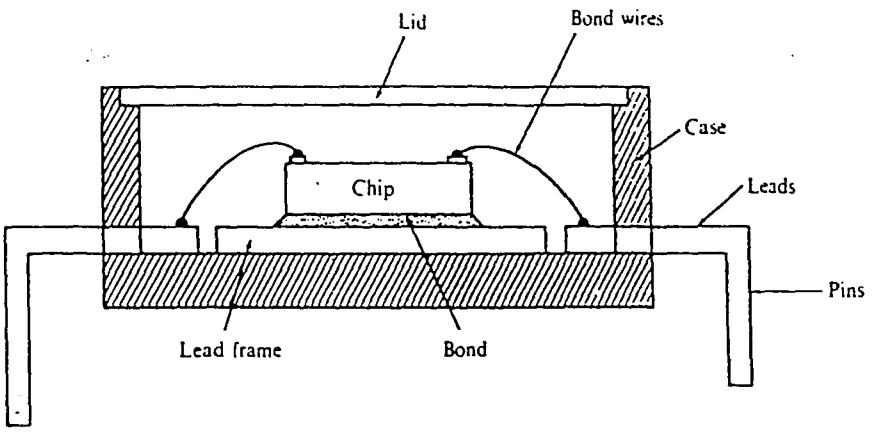

Figure 1.2
A schematic of a typical chip carrier,
[Dally, 1990]

The type of packaging considered in the study is the second level packaging or the PCB. The PCBs serve as mounting places for various electronic components including resistors, diodes, capacitors and integrated circuits (ICs). A completely assembled PCB can have hundreds of such devices. The problem usually faced by designers is to pick the optimum arrangement of those devices to deliver optimum performance and reliability. This problem is difficult to solve because of the very large number of distinct placement possibilities that exist and it is usually not economical to pursue the necessary calculations to find the optimum arrangement.

Regardless of the level of packaging being considered, it is important for the manufacturer to evaluate alternative efficient cooling approaches in order to balance performance and reliability without a significant increase in manufacturing cost.

1.2 RELIABILITY ANALYSIS

As mentioned before, the reliability of electronic equipment is highly dependent on the operating temperature. Reliability can be defined as the ability of a system to continue performing its function to the satisfaction of the user and it is usually quantified as the mean time between failures (MTBF). High MTBF means high reliability. It is estimated that the reliability of a component decreases about 2 percent for every 2° C temperature rise [Chung, 1987]. This problem becomes more urgent as the operating temperature of electronic components increases due to the increase in circuit performance (more heat dissipated from faster chips). The requirement for highly reliable products will be the major issue for electronics manufacturers to consider in order to increase their market share and maintain their competitive edge.

There are two primary objectives of thermal management in electronic equipment [Simon, 1983]. The first objective is to assure that the electronic components are kept within the specified operating temperature limits, the maximum and minimum temperatures that the equipment can operate. This is important since failure to satisfy these temperature limits will lead to failures ranging from logic failure to actual physical damage. The second objective is to keep the temperature distribution in the electronic component within the specified reliability limit that is the optimum operating temperature range. Meeting the second objective is important especially in the long run, since a slight change in operating temperature will greatly affect the failure rate.

The exact relationship between the operating temperature and the failure rate will largely depend on the packaging materials, package configuration and manufacturing processes. One widely used mathematical model to predict approximately the relationship between operating temperatures and the failure rate is the Arrhenius model. According to this empirical model, [Fuqua, 1986],

$$F_t = \frac{R_{fT1}}{R_{fT0}}$$

$$F_t = \mathrm{EXP}\left(\frac{E}{k_1}\left(\frac{1}{T_0} - \frac{1}{T_1}\right)\right) \qquad (1.1)$$

where:

F_t = Temperature related failure rate

R_{fT0} = Rate of failure at reference temperature

R_{fT1} = Rate of failure at T_1

T_0, T_1 = Temperatures (in Kelvin)

k_1 = Boltzman constant; 8.616×10^{-5} eV/ K.

E = Activation energy

This model takes into account the changes in device characteristics resulting from chemical or diffusive processes by utilizing a normalized failure rate. Figure 1.3 shows graphically the relationship between operating temperature and the failure rate. The Arrhenius model originated from the ' experimental activation energy ' that determines the slope of the reaction rate with temperature. A low activation energy means low dependency on temperature and vice-versa. Activation energy is a direct result of every chemical reaction. In an electronic component there are several such reactions occurring simultaneously and each one of those reactions can contribute to the component's failure rate. For general classes of electronic components, the cumulative effects of these various reactions are approximated to be exponentially temperature dependent as shown in Figure 1.3 [Arsenault & Roberts,1980].

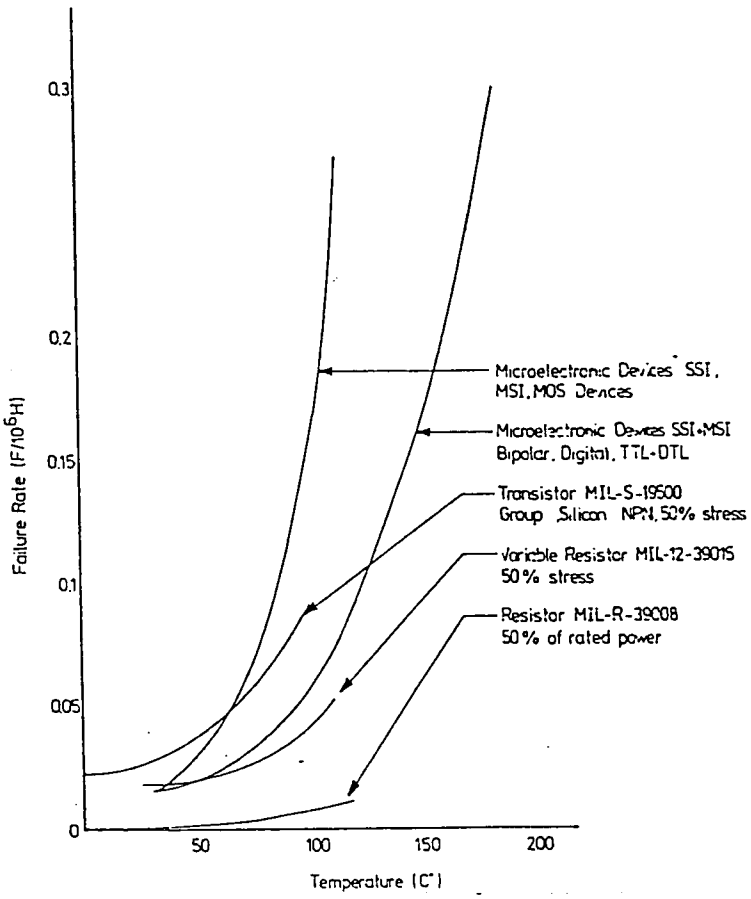

Figure 1.3:
The relationship between temperature and failure rate
[Arsenault & Roberts, 1980]

1.3 Problem Definition

The study of thermal management for second level packaging applications concentrates on the temperature distribution and flow phenomena in air-filled vertical cavities with protruding heat sources. The convective flow in the cavity is calculated for Grashof number ranging from 1×10^2 to 1.5×10^6. The model used in this study is based on the work done by Liakopoulos, et al. [1991] and is shown in Figure 1.4. Both laminar flow and turbulent flow are considered in the study; laminar flow with Grashof number values from 1×10^2 to 7.5×10^5 and turbulent flow with Grashof number values up to 1.5×10^6.

The objective of the current study is to investigate whether flows in tall cavities with periodically spaced protruding heat sources and adiabatic boundary conditions imposed at the upper and lower horizontal walls can be approximated by taking the middle portion and imposing periodic boundary conditions at the upper and lower boundaries. Two geometric cases are considered with the same aspect ratios (height/width), A. The geometry description and the imposed boundary conditions for the two cases considered in this study are shown in Figure 1.5 and Figure 1.6. The chip is modeled as protruding heat source with constant heat flux around the chip surface. The upper and lower boundaries of the computational domain are assumed to be periodic in terms of velocity and temperature. Calculations are carried out to steady state by solving

an initial boundary valued problem with Grashof numbers ranging from zero, the conduction problem, to 7.5×10^5 for the laminar and up to 1.5×10^6 for turbulent flow.

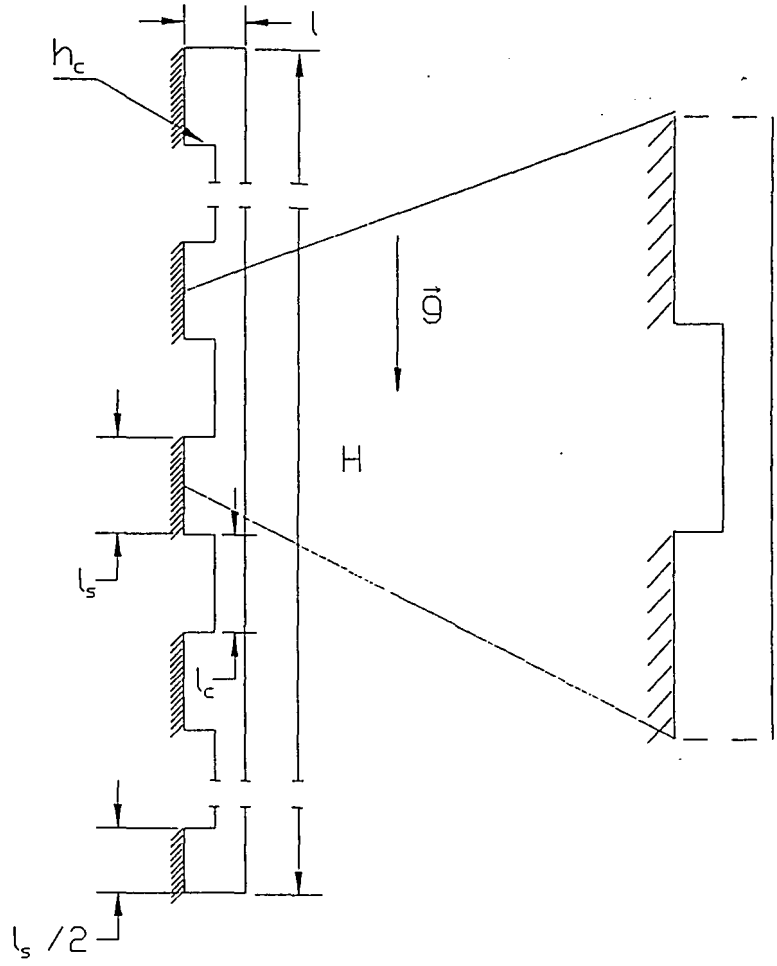

Figure1.4:
Enclosure considered in the study

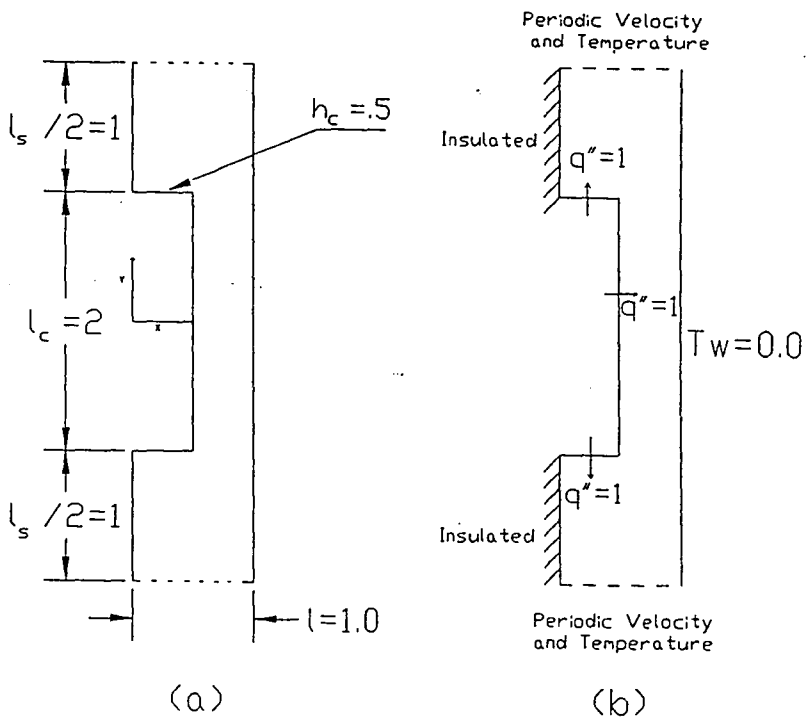

Figure1.5:
Geometric description(a) and imposed boundary conditions (b)

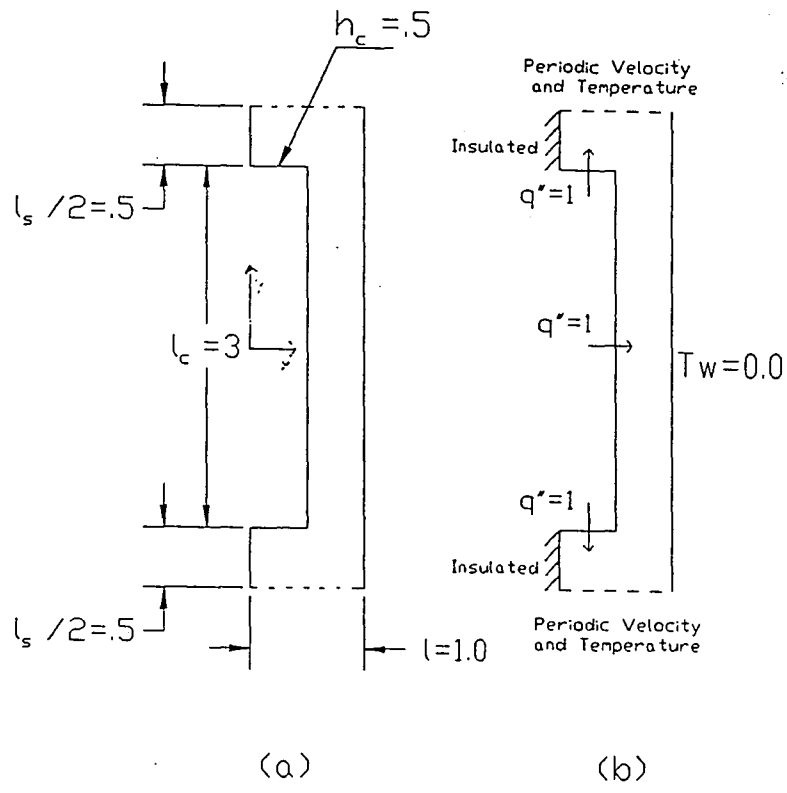

Figure 1.6:
Geometric description (a) and imposed boundary conditions (b) for case 2

1.4 Related Work

Because of the diverse fields in which the study of natural convection within vertical cavities can be applied, there has been much work done in this area either by analytical, computational or experimental methods.

1.4.1 Laminar Flows

As mentioned before, part of this study is based on the work done by Liakopoulos,et al. (1990 and 1991). They investigated the flow caused by natural convection within vertical cavities with periodically distributed flush-mounted heat sources (1990) and uniformly spaced protrusions with surface heating (1991). All flows in their study are assumed to obey the Oberbeck-Boussinesq equations with the effects of viscous dissipation neglected. The governing equations are solved using a spectral element method (Patera, 1984). Their results indicate that the solutions are dependent on the Grashof number, Gr, the cavity aspect ratio, A, the Prandtl number Pr (=.71), and further length scales that characterize the periodic input and protrusion shape. As the Grashof number was increased, significant eddy distortions accompanied by enhancement of the vertical heat flux were observed.

Much experimental work has also been done in natural convection in vertical cavities with protruding heat sources. Kelleher et al. (1987) and Lee et al. (1987) performed experiments with one protruding heat source placed on three different locations in the cavity; bottom, middle and top. Both numerical and experimental results

were presented. Their results indicate that the local Nusselt number (Nu) decreased when the heat source was raised (from bottom to the top) for a given Rayleigh number. Keyhani, Chen and Pitts (1991) conducted experiments with five protruding heat sources placed in a rectangular enclosure to determine the effect of aspect ratio on heat transfer. They used ethylene glycol with Pr=166 as the working medium instead of air. Their results indicate that the velocity of the fluid decreased as the width of the cavity is increased.

1.4.2 Turbulent Flows

There have not been many studies published in this area compared to the laminar cases. One experiment that is closely related to the turbulent flow has been reported by Miyamoto et al. (1986). Miyamoto conducted experiments with two parallel plates arranged vertically; one plate with uniform heating and the other fully insulated. He investigated the temperature distribution on both vertical plates and measured the turbulent quantities. Using the correlation between the two quantities, he then approximated the value for the heat transfer coefficient. A numerical study of bouyancy-induced turbulent natural convection has been done by Cheung et al. (1989). In the study, the flow development and the heat transfer characteristics were investigated in an innovative air cooling system using an implicit finite-difference method.

1.5 Organization of Thesis

In this thesis, the fluid flow and heat transfer in a vertical channel with one protruding heat source are analyzed using the spectral element method. Chapter 1 of this thesis discussed the problem definition and the importance of the current study in terms of improving reliability in electronic equipment. The description of the governing equations and a brief explanation of the spectral element method are presented in chapter 2. The discussion includes the importance of temporal and spatial discretizations for solving the Navier-Stokes equation and the fluid dynamics software package, used in the current study. The numerical results and discussion are presented in chapter 3 with emphasis on fluid flow phenomena and heat transfer. Both aspects are analyzed with respect to the increase in the Grashof number. Finally, the conclusions and recommendations for future works are presented in chapter 4.

CHAPTER TWO

MATHEMATICAL MODEL & SOLUTION METHOD

2.1 Governing Equations

In this study, all flows are assumed to be two dimensional and the convective motion is governed by the Boussinesq approximation, i.e. density changes are significant only in the body force term in the momentum equation.

The governing equations for flows in vertical channels are as follows:

the continuity (mass conservation) in D_F,

$$\frac{\partial u}{\partial x}+\frac{\partial v}{\partial y}=0 \tag{2.1}$$

the momentum equation in D_F,

$$\rho(\partial_t \vec{V}+(\vec{V}\cdot\nabla)\vec{V})=-\nabla p+\nabla\cdot\left[\mu(\nabla\vec{V}+(\nabla\vec{V})^T\right]-\rho\bar{\beta}T\vec{g}+\rho\vec{f} \tag{2.2}$$

the energy equation in D_F,

$$\rho C_p\left[\partial_t T+(\vec{V}\cdot\nabla)T\right]=\nabla\cdot(k\nabla T)+q_{vol}+\mu\nabla\vec{V}:(\nabla\vec{V}+\nabla\vec{V}^{T}) \qquad (2.3)$$

where D_F is the fluid domain.

Equations (2.1) - (2.3) are non-dimensionalized by introducing dimensionless variables as follows :-

$$\vec{v}=\frac{\alpha}{l}\vec{v^*} \quad , \qquad p=\rho_0\frac{\alpha^2}{l^2}p^* \, , \qquad T-T_r=\frac{q''l}{k}T^* ,$$

$$t=\frac{l^2}{\alpha}t^* \quad , \qquad (x,y)=l(x^*,y^*). \qquad (2.4)$$

The resulting dimensionless conservation equations neglecting viscous dissipation and internal heat generation are:

$$\nabla\cdot\vec{v^*}=0 \qquad \text{(continuity)} \quad (2.5)$$

$$\frac{D\vec{v^*}}{Dt}+\nabla p^*=\mathrm{PrRa}T^*\vec{j}+\mathrm{Pr}\nabla^2\vec{v^*} \qquad \text{(Momentum)} \quad (2.6)$$

$$\frac{DT^*}{Dt}=\nabla^2T^* \qquad \text{(Energy)} \quad (2.7)$$

where :

$\frac{D(\bullet)}{Dt}$ denotes the substantial derivative of the physical quantity appearing inside the parenthesis,

$\mathrm{Pr} = \frac{\nu}{\alpha}$ denotes the Prandtl number,

and $\mathrm{Ra} = \frac{\beta g \Delta T L^3}{\nu \alpha}$ denotes the Raleigh number.

In each case, the right wall is assumed to be at constant temperature whereas periodic boundary conditions for velocity and temperature are imposed at the upper and lower boundaries of the computational domain as shown in Figures 1.5 (b) and 1.6 (b). The origin of the Cartesian coordinate is shown in Figures 1.5 (a) and 1.6 (a). Fluid motion is generated by protruding heat sources of uniform heat flux mounted on the left vertical wall.

The imposed boundary conditions for all cases are as follows:

- Flow boundary conditions

  (a) No slip boundary conditions are imposed at each wall,

  $$u^* = v^* = 0$$

  (b) Periodic velocity at $y^* = -2$ and $y^* = 2$

- The thermal boundary conditions are (refer to Figure 1.5(b) and 1.6(b)) :

a) Periodic in terms of temperature at lower (y*= -2) and upper boundary (y*=2).

b) Adiabatic (thermally insulated) : $\frac{\partial T^*}{\partial x^*} = 0$ at

case 1			case 2		
x*=0	and	$1 \le y^* \le 2$	x*=0	and	$1.5 \le y^* \le 2$
		$-2 \le y^* \le -1$			$-2 \le y^* \le -1.5$

c) Uniform heat fluxes: q"=1 at

case 1			case 2		
y*=1	and	$0 \le x^* \le .5$	y*=1.5	and	$0 \le x^* \le .5$
y*=-1	and	$0 \le x^* \le .5$	y*=-1.5	and	$0 \le x^* \le .5$
x*=.5	and	$-1 \le y^* \le 1$	x*=.5	and	$-1.5 \le y^* \le 1.5$

d) Isothermal, T*= 0 at

x*=1 and $-2 \le y^* \le 2$ for both cases

2.2 Numerical Procedure

The mathematical models are solved using a spectral element method (Patera 1984). The approach uses a time-accurate integration scheme, and consequently, it is possible to distinguish between time-independent and oscillatory asymptotic states.

2.2.1 Spatial Discretization

The computational domain is divided into M non-overlapping macro-elements. Within each macro-element, the unknown functions $\vec{V}(x,y,t)$, p(x,y,t) and T(x,y,t) are approximated by Legendre polynomials of order (N-1) that interpolate in each spatial direction the unknown functions at the N Gauss-Lobatto-Legendre collocation points (Patera, 1984). Continuity of the functions $\vec{V}$, p, and T at the interfaces between macro-elements is imposed. However, continuity of the derivatives at the interfaces is achieved only when numerical solutions converge to the exact solutions. Algebraic rates of convergence, similar to low-order finite-element or finite-difference techniques, are achieved by increasing the number of macro-elements, M while exponential rates of convergence are achieved by increasing the N, which is the order of the interpolating Legendre polynomial. Typically, in the computations N varies from 5 to 9. A more detailed discussion concerning the optimal selection of M and N can be found in Fischer et al. (1988).

2.2.2 Temporal Discretization

The non-linear convective terms and the body-force terms are integrated in time by an explicit third-order Adams-Bashforth scheme, but the diffusion terms are treated implicitly using the Euler backward method. Although the implicit treatment of the diffusion terms does not impose any restrictions on the time step Δt, the explicit treatment of the convective terms requires that Δt is small enough in order to satisfy the numerical stability so that the Courant number, $Co \leq Co_{cr}$ where

$$Co = \max_{D}\left(\Delta t \frac{u}{\Delta x}, \Delta t \frac{v}{\Delta y}\right)$$

and $\max_D$ refers to the maximum over the entire flow field. The critical Courant number, Co_{cr}, has to be less than 0.71 for the split-formulation.

2.2.3 Formulation and Solution of Discrete Equations

All high Rayleigh number computations are performed using time-split formulation (Yanenko, 1971). At low Rayleigh number, solutions are computed using Uzawa's algorithm. This eliminates the splitting errors that can arise at speed characteristic of small Rayleigh number flows. In every case the discrete equations are solved by the conjugate gradient method (Canuto et al., 1988).

2.2.4 NEKTON

All the numerical solutions in the current study were preformed on several mainframes and workstations; VAX 8530, IBM RS/6000 model 950 and Stardent P3000 superworkstation. The software package NEKTON, designed for steady and unsteady fluid flow and heat transfer as well as convective-diffusive passive scalar transport, has been used for the numerical solution. The numerical procedure in NEKTON is based on a spectral element method. In addition, the program spectralview developed by Huang and Liakopoulos (1991) was used for computer flow visualization and data analysis.

Transitions from the base flow are studied by gradually increasing the Rayleigh number or equivalently the Grashof number,

$$Gr = \frac{\mathrm{Ra}}{\mathrm{Pr}} = \frac{\beta g q'' l^4}{\nu^2 \alpha k}.$$

In this study the results are presented in terms of Gr.

The computational domain for all cases is divided into macro-elements in which a local Cartesian mesh is constructed by mapping the physical (x,y) space to a local (r,s) coordinate system. The convergence to the exact solution depends on the size of the macro-element and the order of the interpolant used. By increasing the number of macro-elements, the error (compared to the exact solution) will decrease with the mesh size Δx. On the other hand, the error will decrease exponentially if the order of

interpolant is increased. In this study the order of interpolant used was 5 for low Grashof number, 7 and 9 for high Grashof number. For example, for Gr=1 x 10^5 , N of 9 was used.

CHAPTER THREE

Numerical Results

The flow phenomena and heat transfer due to natural convection in a vertical channel with protruding heat sources are investigated for two different geometries. The two geometries have the same aspect ratio, $h/l = 4$, but they have different chip height (protruding heat source) and therefore different values of total heat dissipated. The flow and heat transfer phenomena are examined for both laminar and turbulent flows. The Grashof numbers considered in the study range from zero (conduction) to 1.5×10^6.

The calculations are carried out for large values of time, $t \rightarrow \infty$, until steady state solution is achieved. The steady state solution can be time-independent (steady), time-dependent (periodic), or chaotic for laminar flow, and time-independent for turbulent flow. In the subsequent sections, the results and discussion of steady state solutions are presented for different Grashof numbers. The discussion of results is divided into two categories depending on the flow regime; laminar and turbulent.

In order to assure the accuracy of the presented numerical results, a useful check is used where the energy balance for the entire cavity is considered. Since the upper and lower boundaries are periodic in terms of temperature and velocity, the resulting enegy balance equation is as follows:

$$q_L = k\int_{-2}^{2}\left[\frac{\partial T^*}{\partial x^*}\right]_{leftwall} dy^* = k\int_{-2}^{2}\left[\frac{\partial T^*}{\partial x^*}\right]_{rightwall} dy^* = q_R$$

The residuals $q_L - q_R$ for various values of Grashof numbers are presented in Table 3.1

Grashof Number	ql-qr	
	Case 1	Case 2
0	0.000	0.000
100	0.000	0.020
1,000	0.006	0.049
10,000	0.007	0.060
100,000	0.084	0.092
200,000	0.085	0.013
300,000	0.022	0.012
400,000	0.016	0.013
500,000	0.013	0.079

Table 3.1

3.1 Laminar Flows

The discussion of results for laminar flows concentrates on the changes in the flow and heat transfer behavior as the Grashof number is increased.

3.1.1 First case Geometry: $\frac{l_c}{l} = 2$

The first case geometry is investigated for Grashof number ranging from zero (conduction) to 7.5 x 10^5. The steady state solutions for this case indicate that the flow and temperature fields can be time-independent, time-periodic and chaotic. Plots for isotherms, streamlines, vorticity contours and isobars are presented in Figures 3.1, 3.2, 3.3, and 3.4 for selected Grashof numbers. Figure 3.5 shows how the local Nusselt number changes as the Grashof number is increased.

$$Gr < 1 \times 10^4$$

At low Grashof numbers, i.e. Gr < 1 x 10^4, the steady state solutions exhibit the same behavior as that of conduction in terms of maximum temperatures and isotherm patterns. This means that in this range of Grashof numbers, buoyancy forces are very weak and therefore the heat removal from the system due to natural convection is negligible. Referring to the streamfunction, ψ, contours (Figure 3.2), for low Grashof numbers, a large eddy is formed in the cavities between the protruding elements. On the other hand, the flow above the heating element is undisturbed and the streamlines are parallel to the vertical walls.

$$10^4 \leq Gr < 3 \times 10^5$$

In this range, the maximum non-dimensional temperature (T^*_{max}) is reduced significantly. For example, referring to Figure 3.6, T^*_{max} is reduced as much as 30 percent as the Grashof number is increased from 1×10^4 to 3×10^5. In this Grashof number range, the steady state solutions are still time independent. The flows, as shown in the streamline plots, become more unstable characterized by elongation of the large eddies in the cavities between the heating elements.

$$3x10^5 \leq Gr \leq 5x10^5$$

As the Grashof number is further increased to a range of 3×10^5 and 5×10^5, the steady state solutions become oscillatory and periodic in time. For this case, with aspect ratios $h/l = 4$, $h_c/l=0.5$ and $l_c/l=2$, the Grashof number of 3×10^5 becomes the Gr_c where the first instability occurs in the flow. The velocity and temperature fields are oscillating periodically in time while laminar flow behavior is maintained. As one can see from the streamlines plots, the elongated eddies in the cavities between the heating elements are now separated forming two smaller eddies. The eddies above the heating element are also become stronger and more elongated. The cooling enhancement for this range of Grashof number in terms of T^*_{max} shows improvement of about 43 percent relative to the conduction solution (refer to Figure 3.6).

The results for time dependent flows are presented in phase plane plots of temperature versus x-velocity (Figure 3.7). All the phase plots indicate that the steady

state solutions are in fact time periodic. Shown in Figure 3.8 are frequencies calculated using Fast Fourier Transform (FFT) analysis. The results of the analysis indicate that the frequency of oscillation increases with Grashof number. Figure 3.9 represents the instantaneous patterns of isotherms and streamlines during one cycle of oscillation for Grashof number of 5×10^5. As one can see, the distortions of isotherms above the heating element move downward and the eddies are slowly formed above the heating element as the cycle progresses.

$$Gr > 5x10^5$$

For Grashof numbers above 5×10^5, the steady state solutions are no longer time periodic; instead they start to exhibit chaotic behavior. This condition can be seen from the FFT analysis where the results indicate that there exists a large number of frequencies, both harmonic and subharmonic. In other words, the steady state solutions are not periodic - as pointed by the phase plots. The results from the FFT analysis and the phase plots are presented in Figures 3.10 and 3.11 respectively. Isotherms, streamfunction and vorticity contours are presented in Figure 3.12.

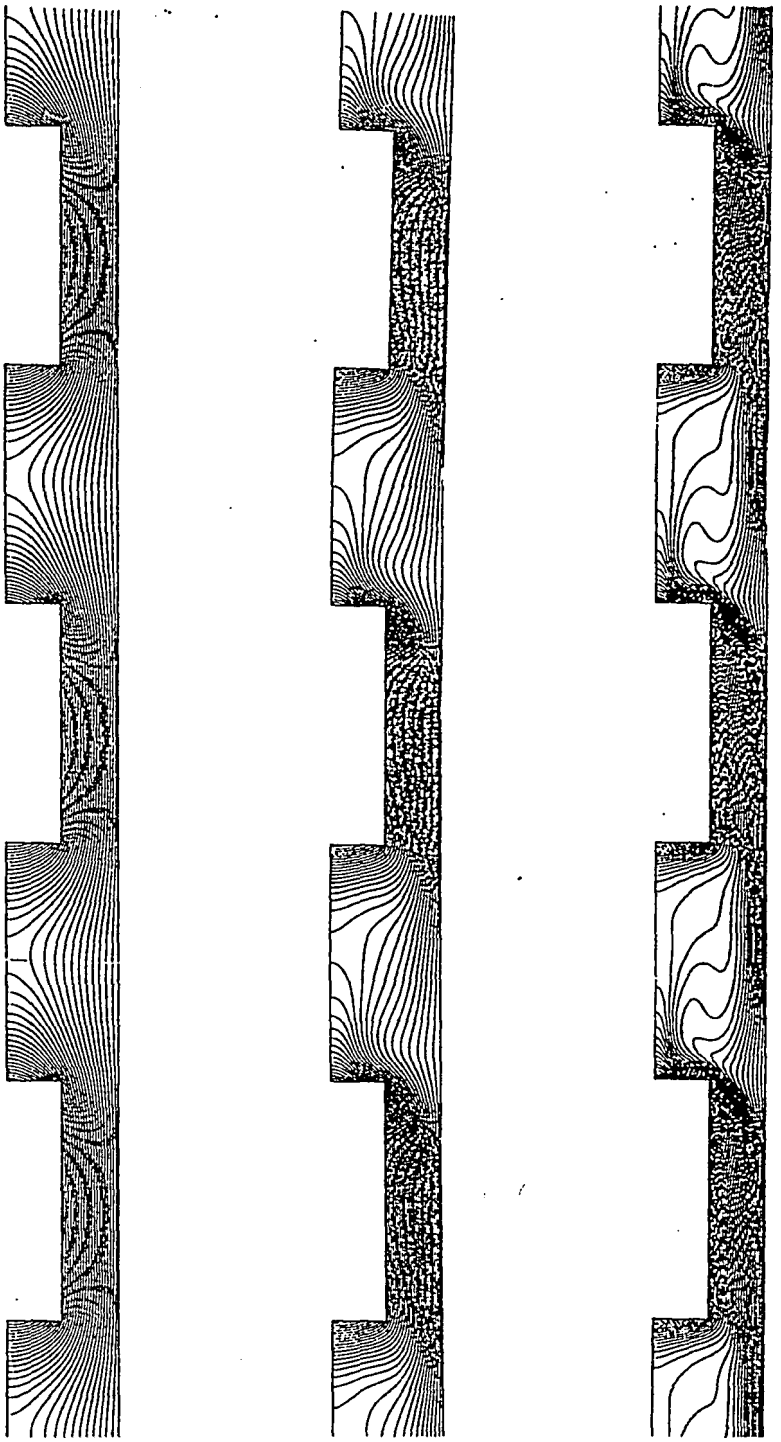

Gr=1000 Gr=$1x10^4$ Gr=$1x10^5$

Figure 3.1 :
Isotherms for case 1

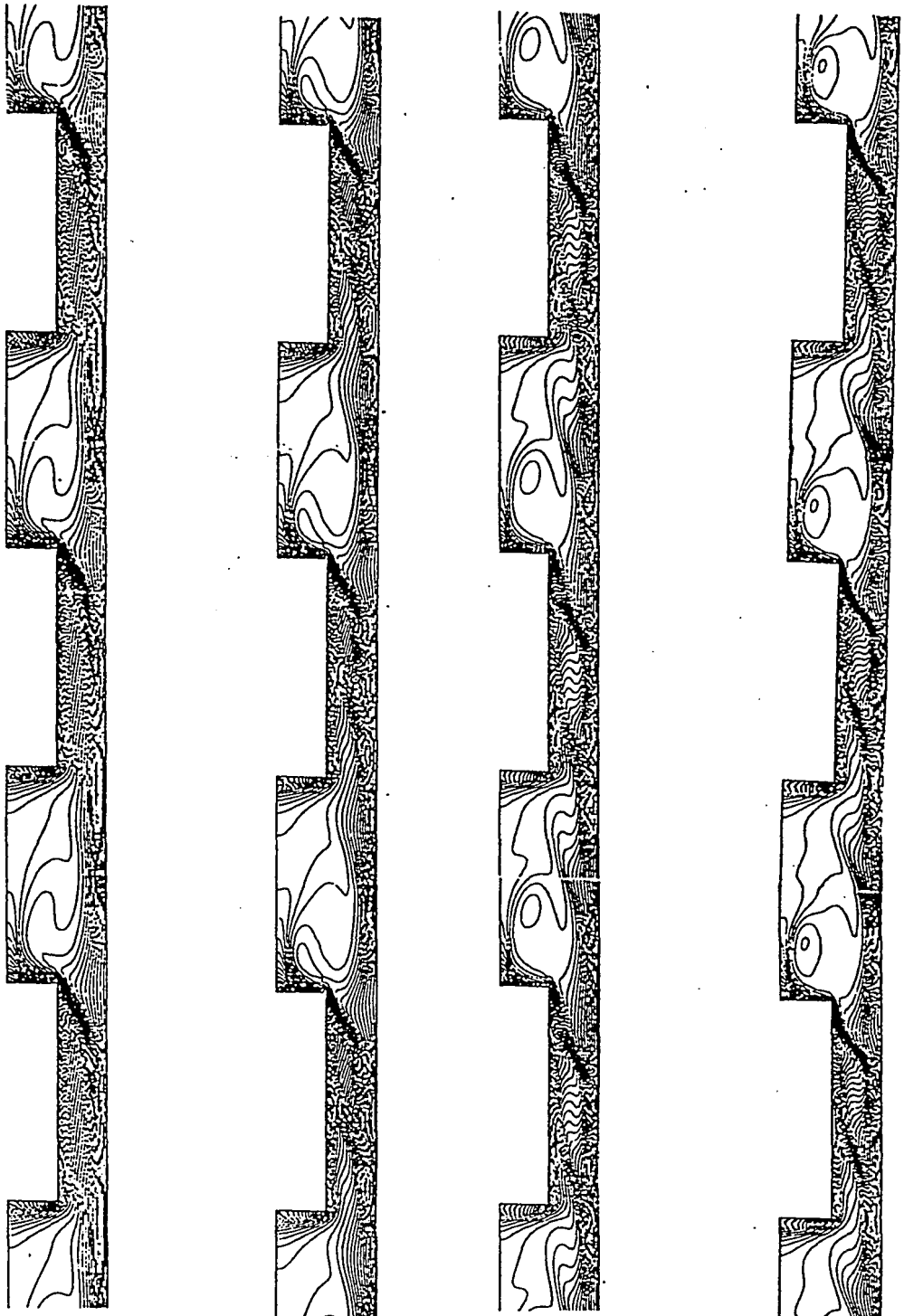

Figure 3.1(cont'd) :
Isotherms for case 1

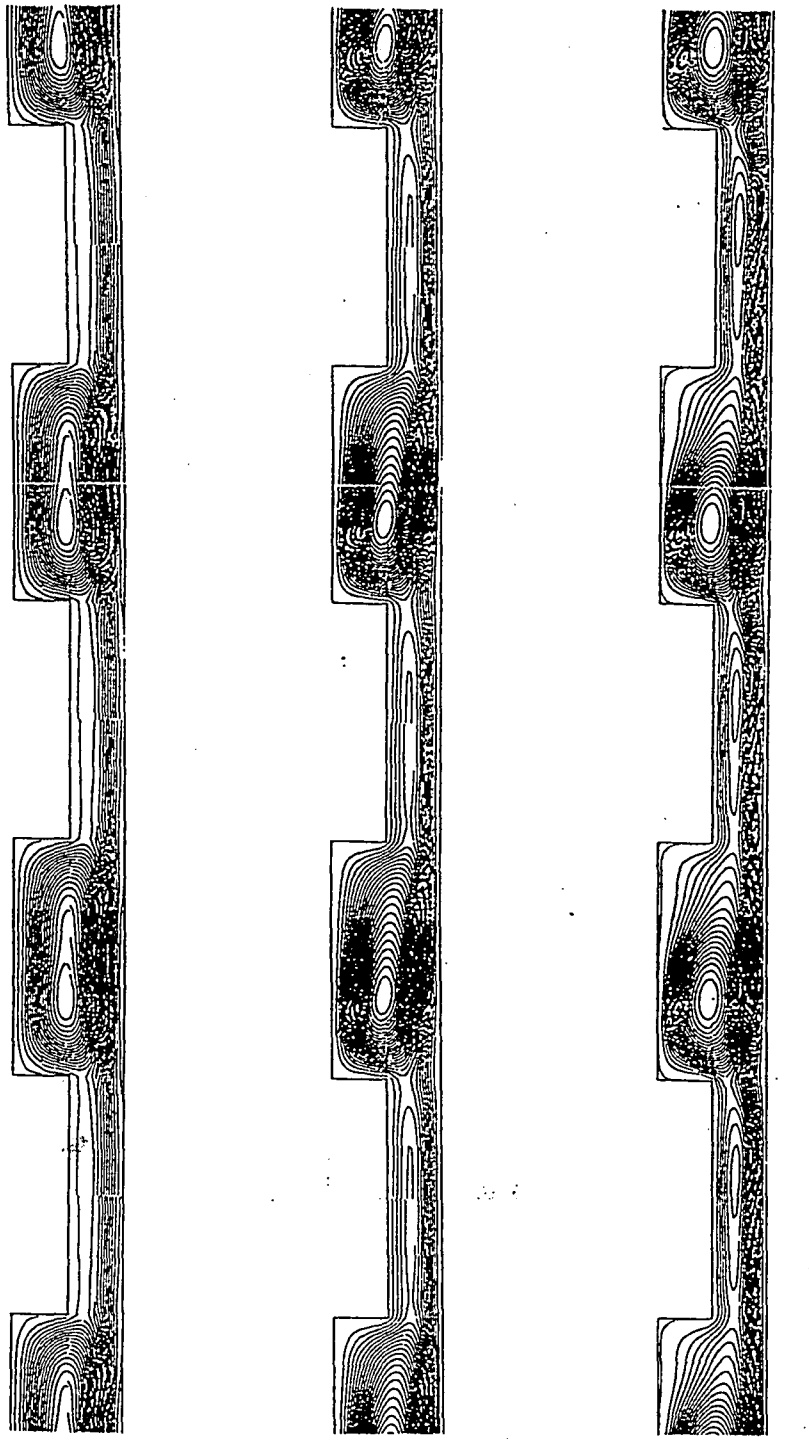

Gr=1000 Gr=1x10^4 Gr=1x10^5

Figure 3.2 :
Streamlines for case 1

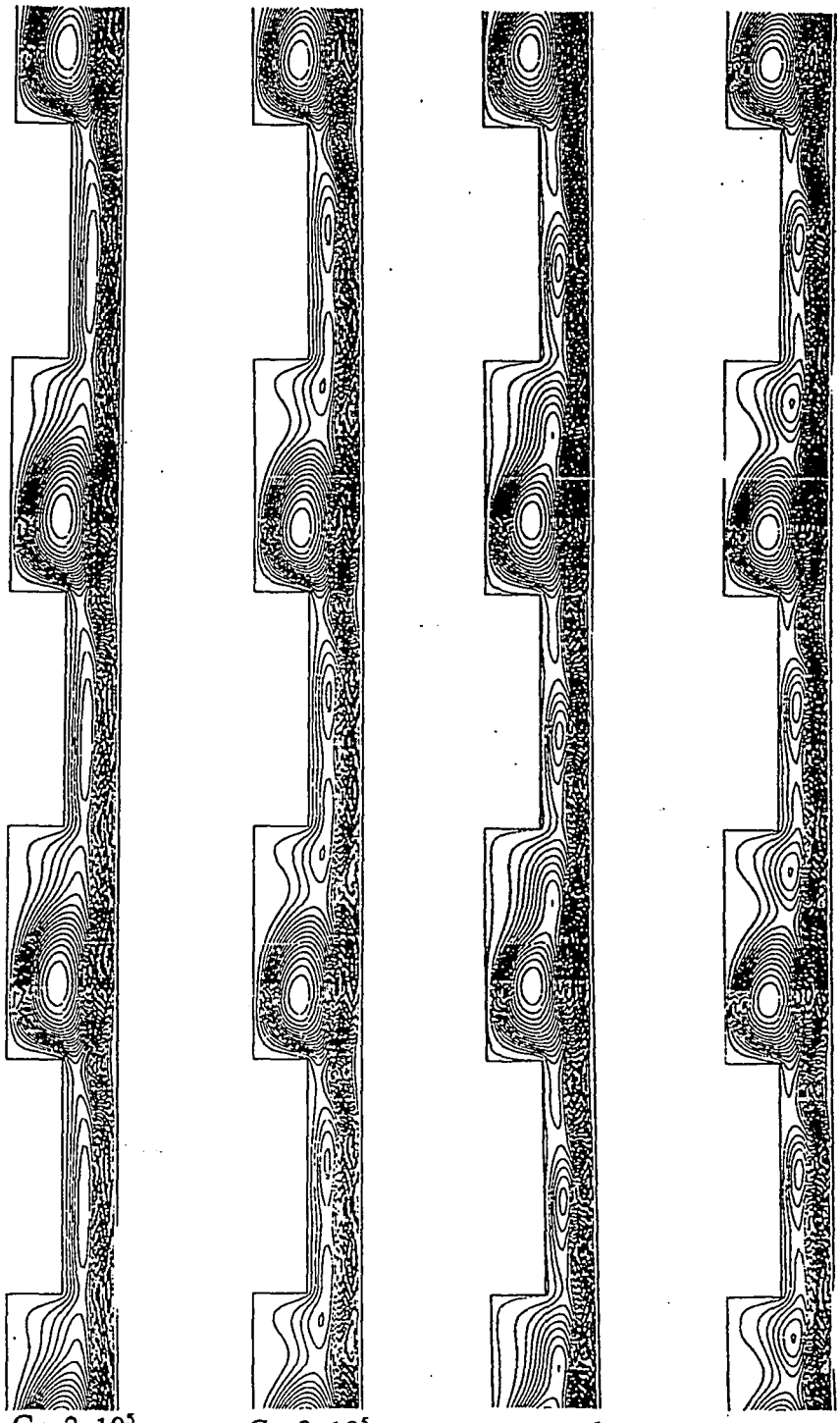

Figure 3.2(cont'd) :
Streamlines for case 1

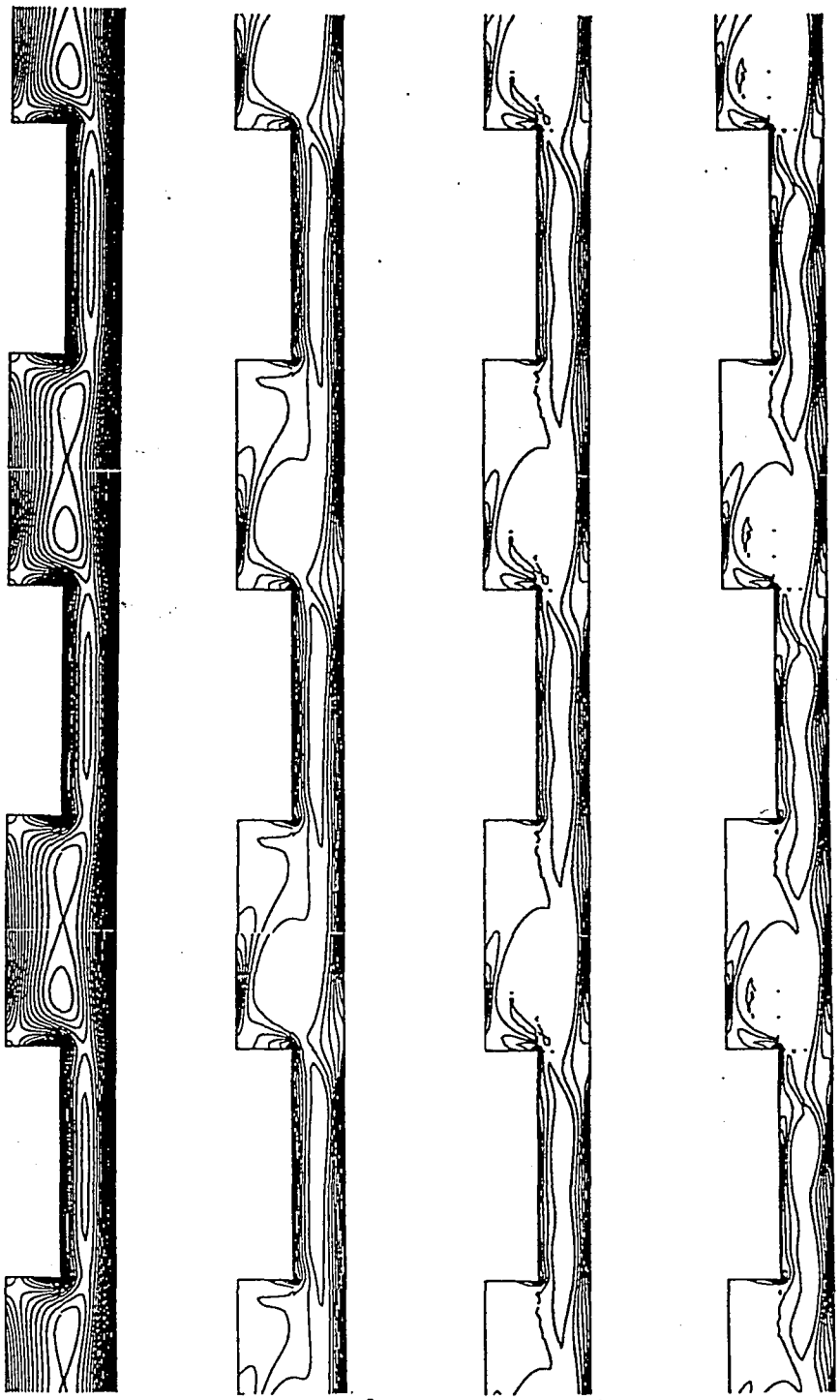

Figure 3.3 :
Vorticity contours for case 1

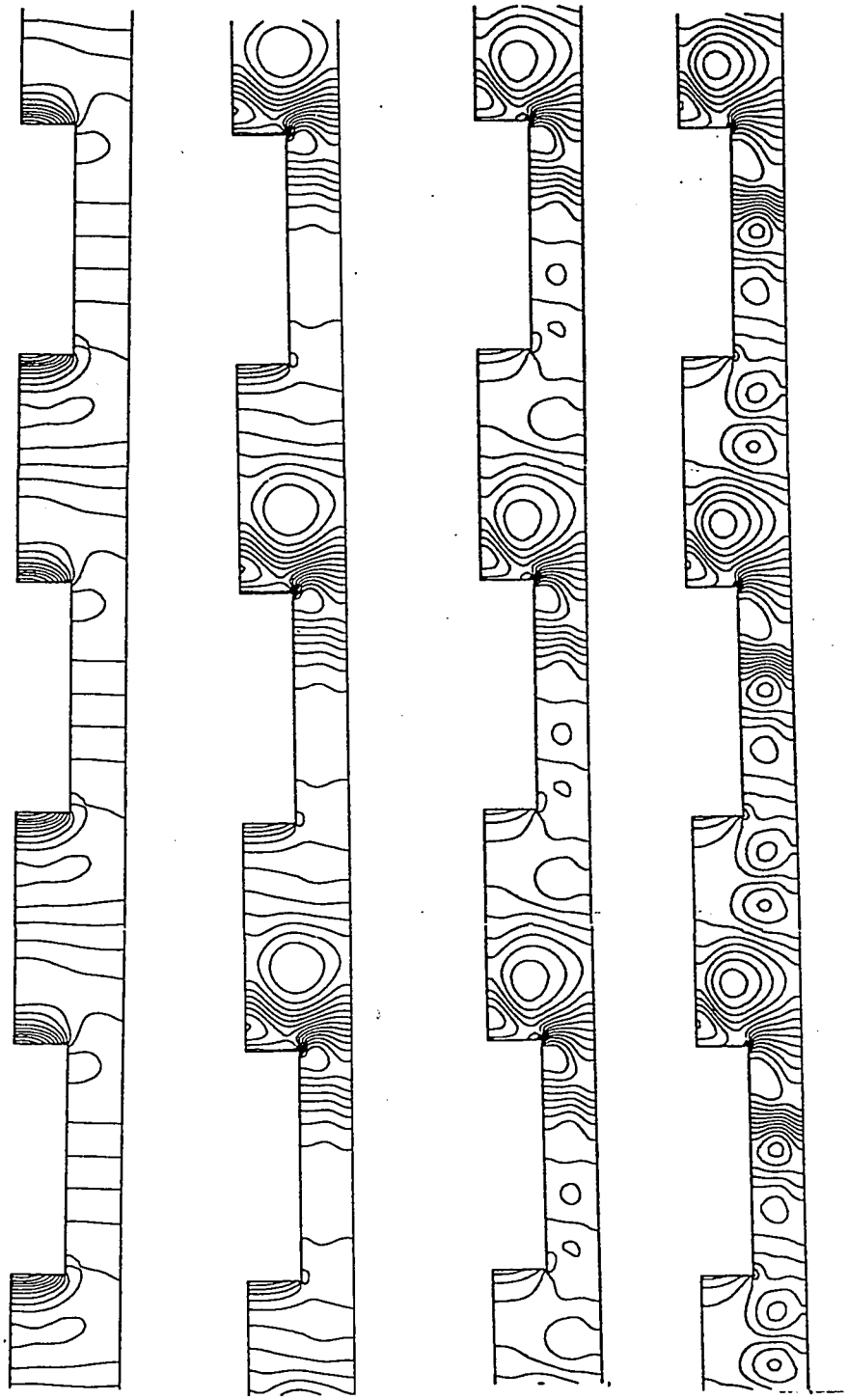

Figure 3.4 :
Isobars for case 1

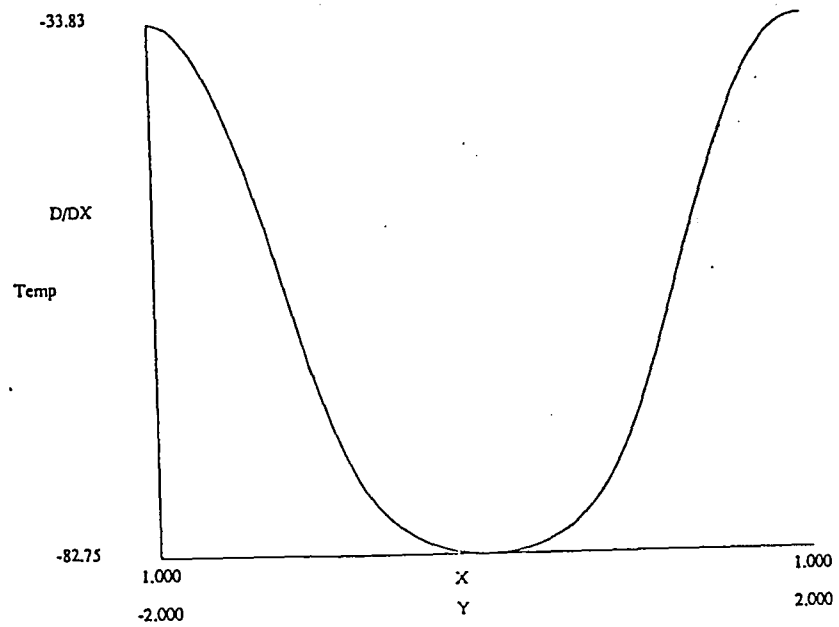

(a)

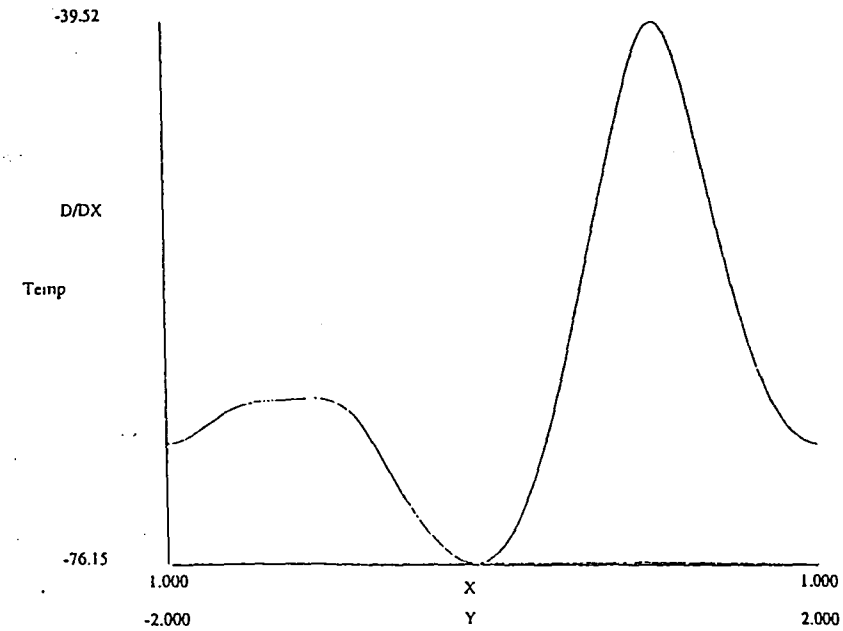

(b)

Figure 3.5:
Plot $\partial T^*/\partial x^*$ at $x^*=1$ and $-2<y^*<2$
(a) Gr=100; (b) $Gr=2x10^5$

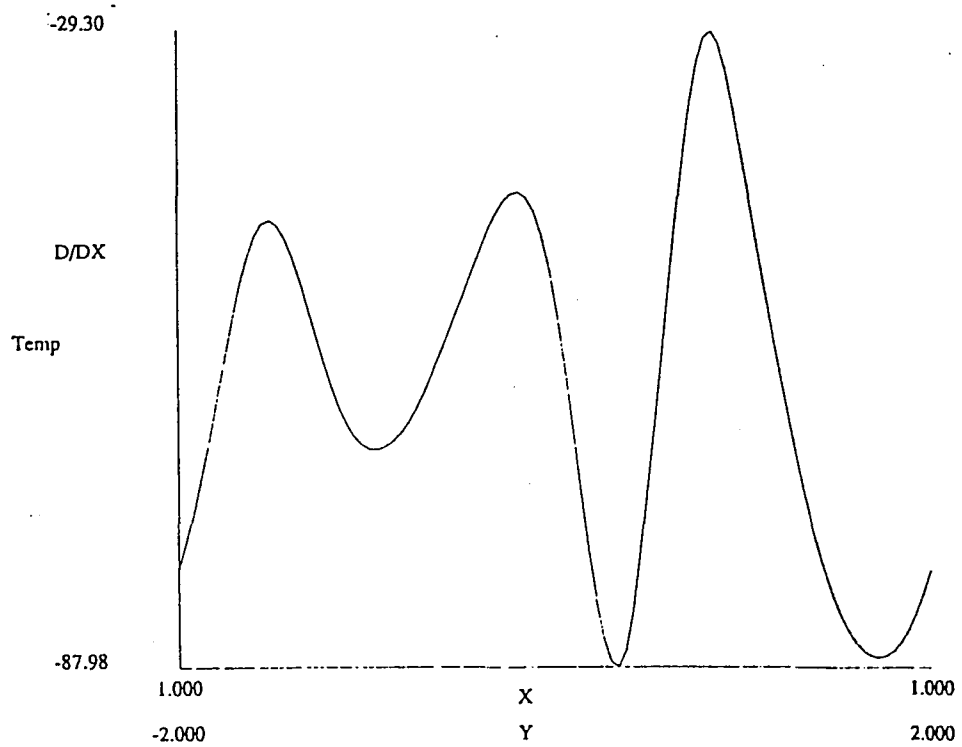

(c)

Figure 3.5 (cont'd):
Instantaneous $\partial T/\partial x$ at $x^*=1$ and $-2<y^*<2$
(c) $Gr=5x10^5$

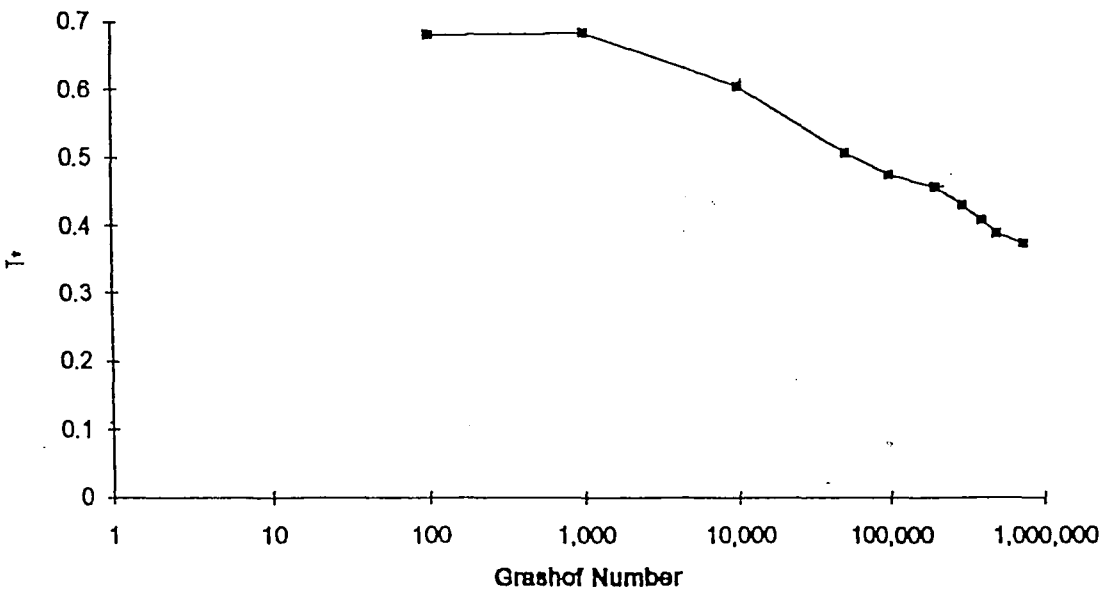

Figure 3.6:
Dimensionless maximum temperature, T^*_{max} vs Grashof number, case 1

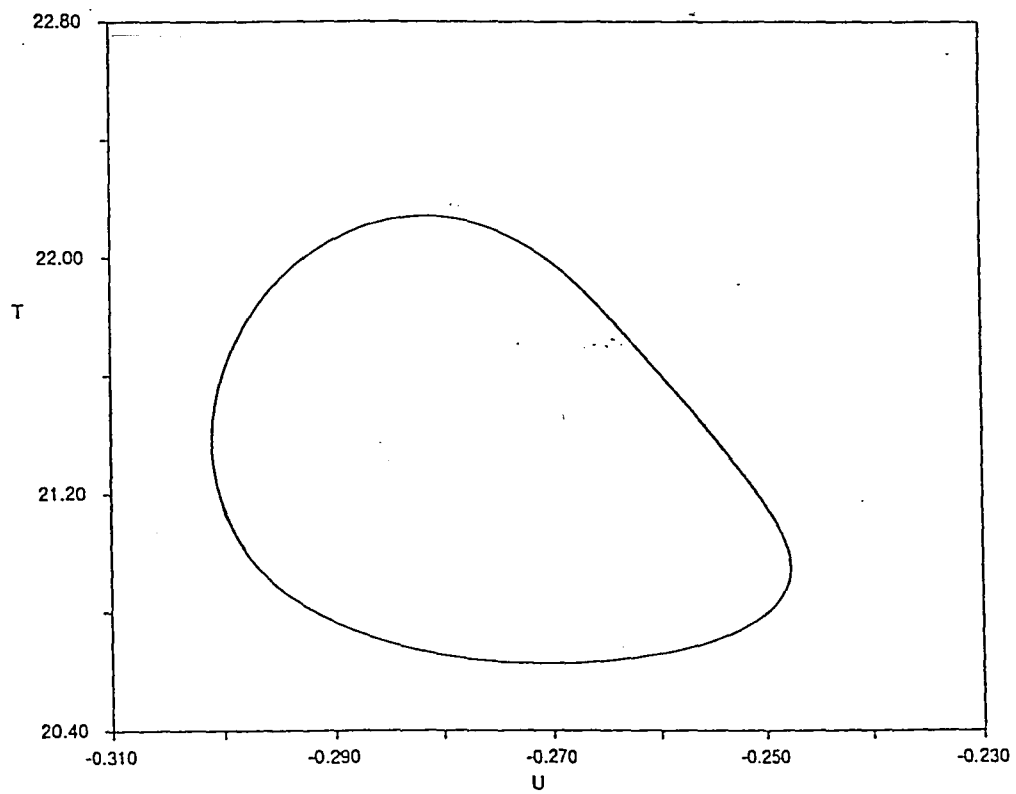

Figure 3.7 :
Phase Plots for Gr=3 x 10^5 , case 1
Temperature vs x-velocity
x* =.75, y* =0

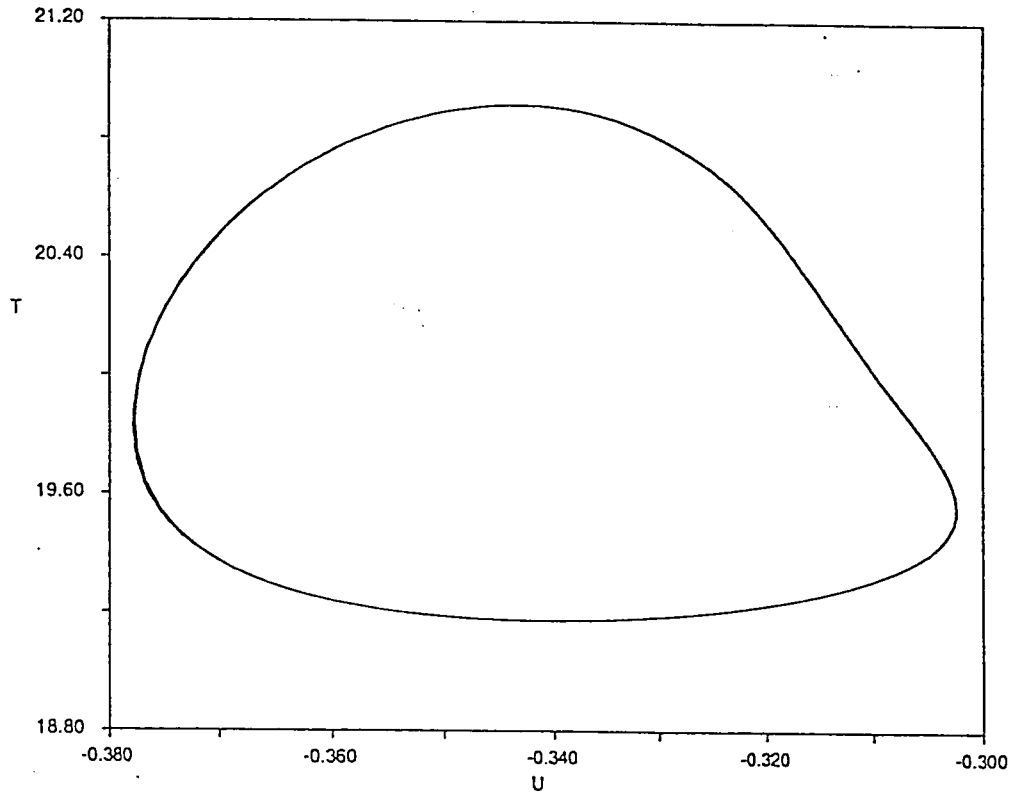

Figure 3.7(cont'd) :
Phase Plots for Gr=4 x 10^5:
Temperature vs x-velocity
x* =.75, y* =0

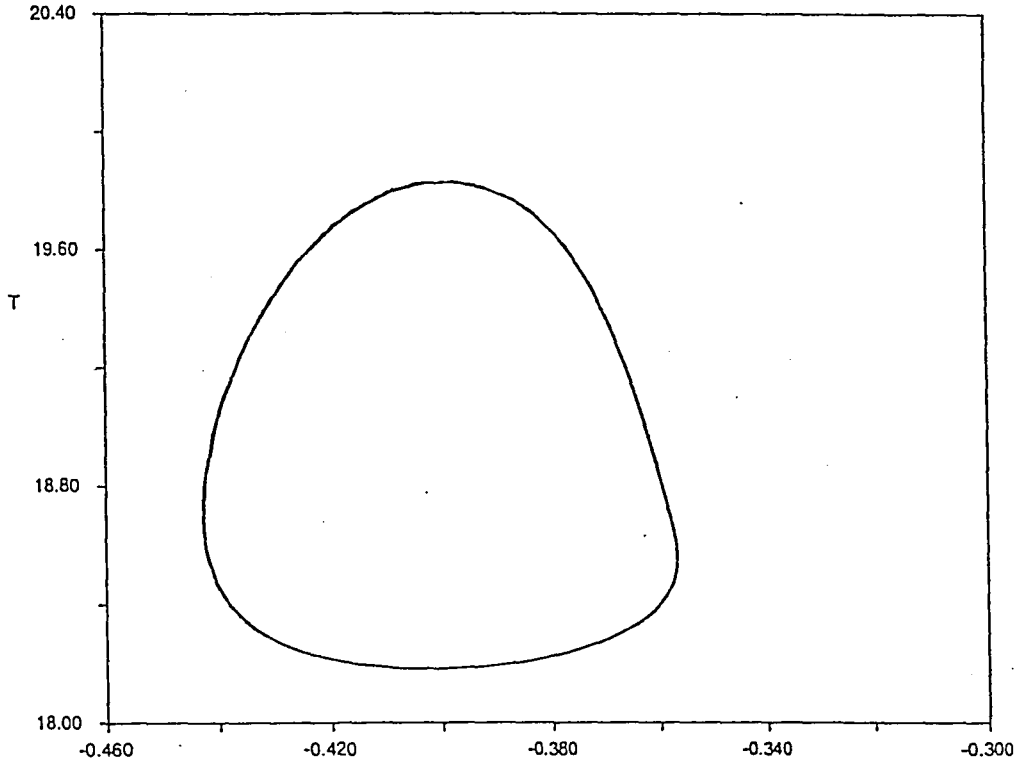

Figure 3.7 (cont'd):
Phase Plots for Gr=5 x 10^5:
Temperature vs x-velocity
x* =.75, y* =0

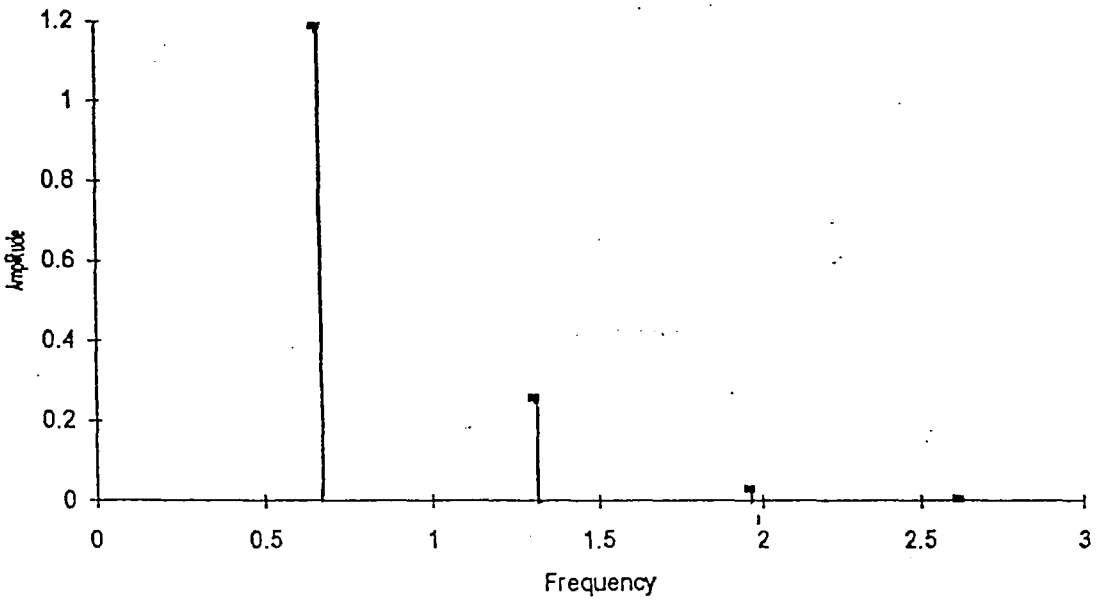

(a)

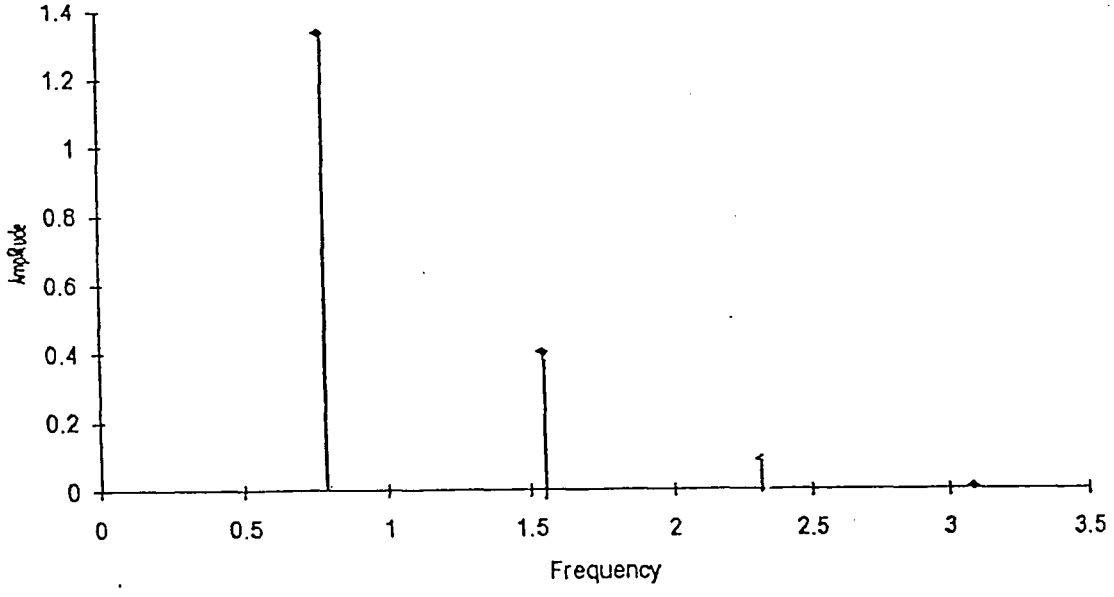

(b)

Figure 3.8:
FFT Analysis of temperature for case 1
(a) Gr=3 x 10^5; (b) Gr=4 x 10^5
x* = 0.75, y* =0

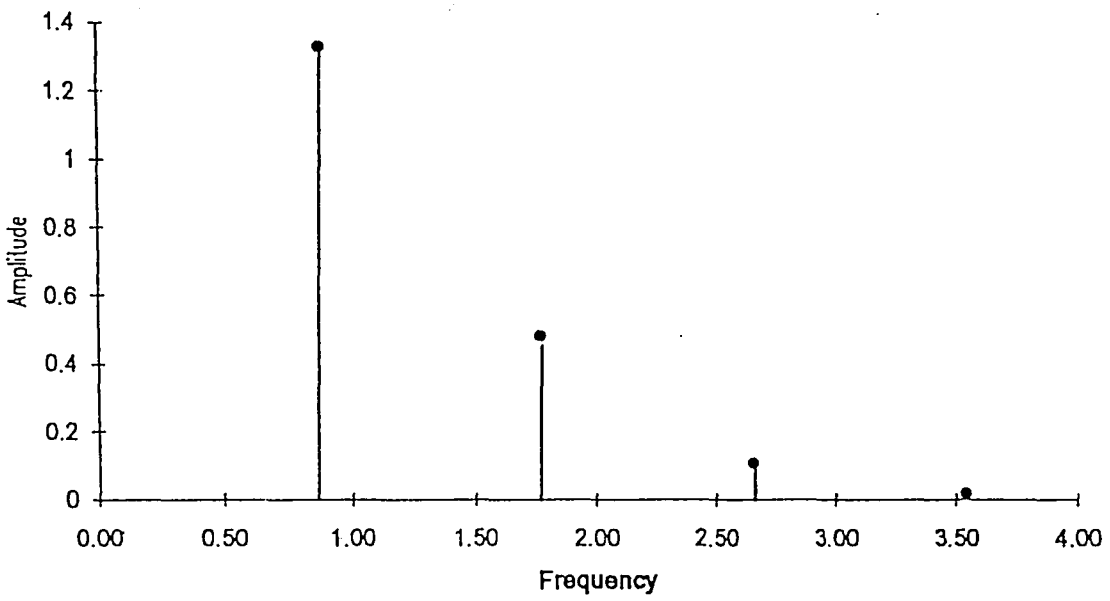

Figure 3.8 (cont'd) :
FFT Analysis of temperature for case 1
Gr=5 x 10^5
x* =0.75, y* = 0

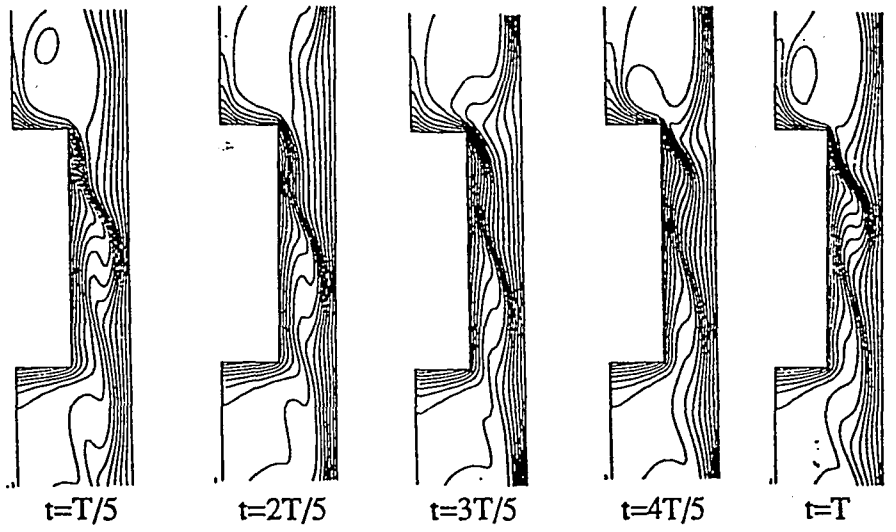

(a)

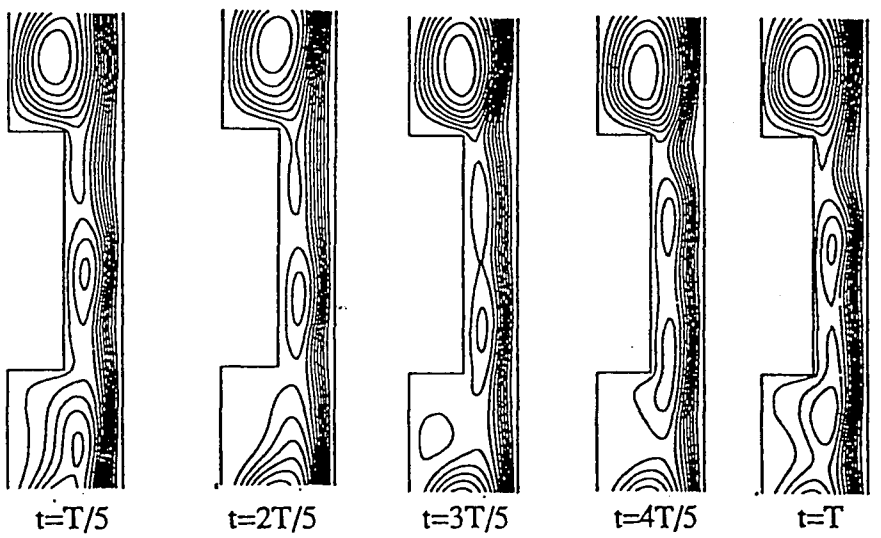

(b)

Figure 3.9 :
Plots for Instantaneous
(a) Isotherms; (b) Streamlines
for Gr =5 x10^5

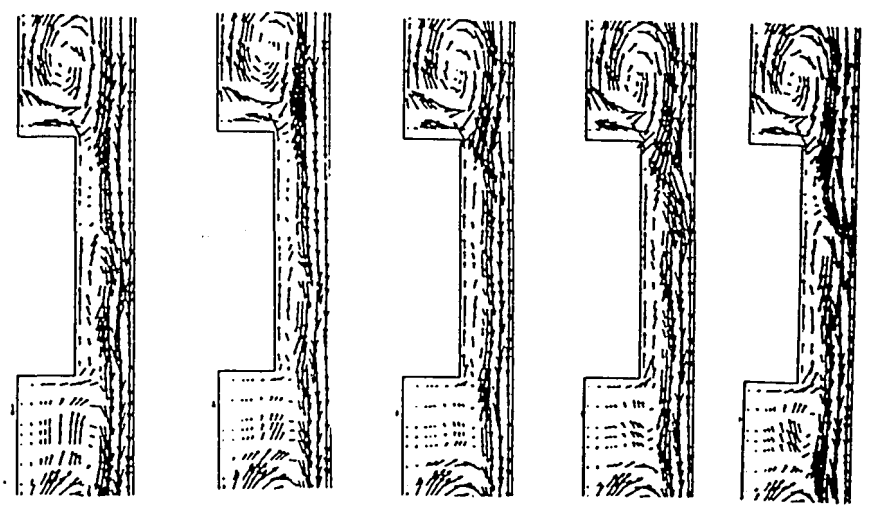

(c)

Figure 3.9 (cont'd) :
Plots for instantaneous
(c) velocity vectors
for Gr = 5×10^5

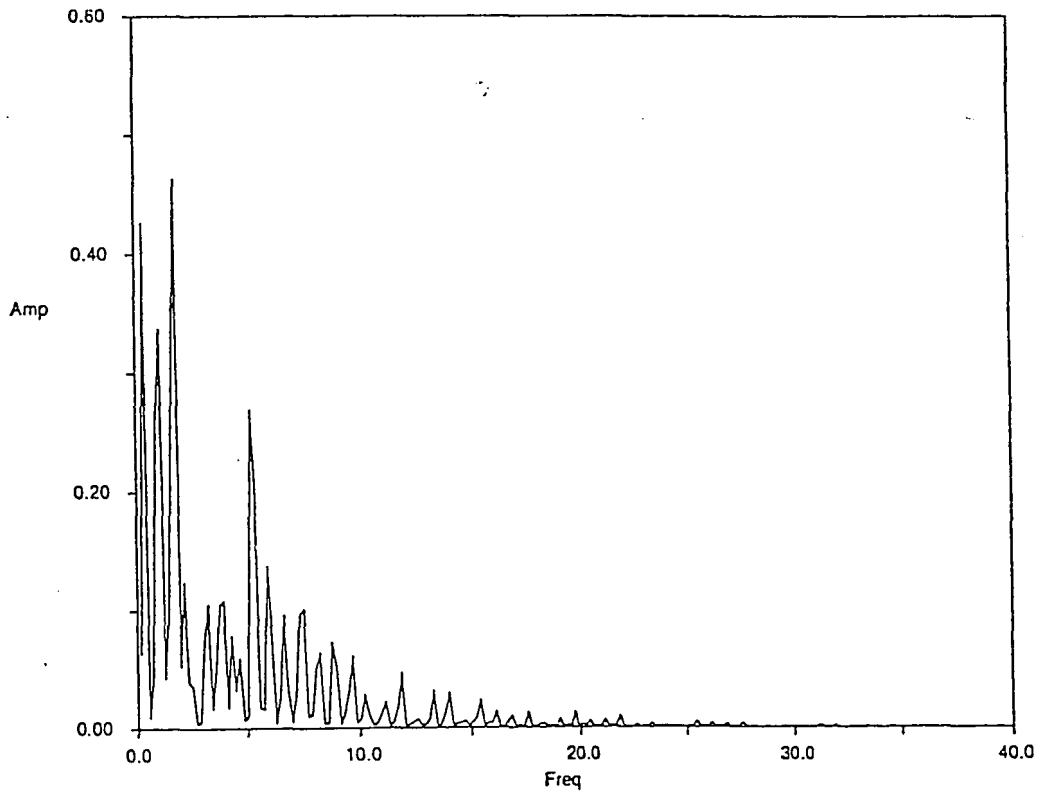

Figure 3.10 :
FFT analysis of pressure for $Gr=7.5x10^5$
at $x^* =0.75$, $y^*=0$
Case 1, chaotic behavior in time

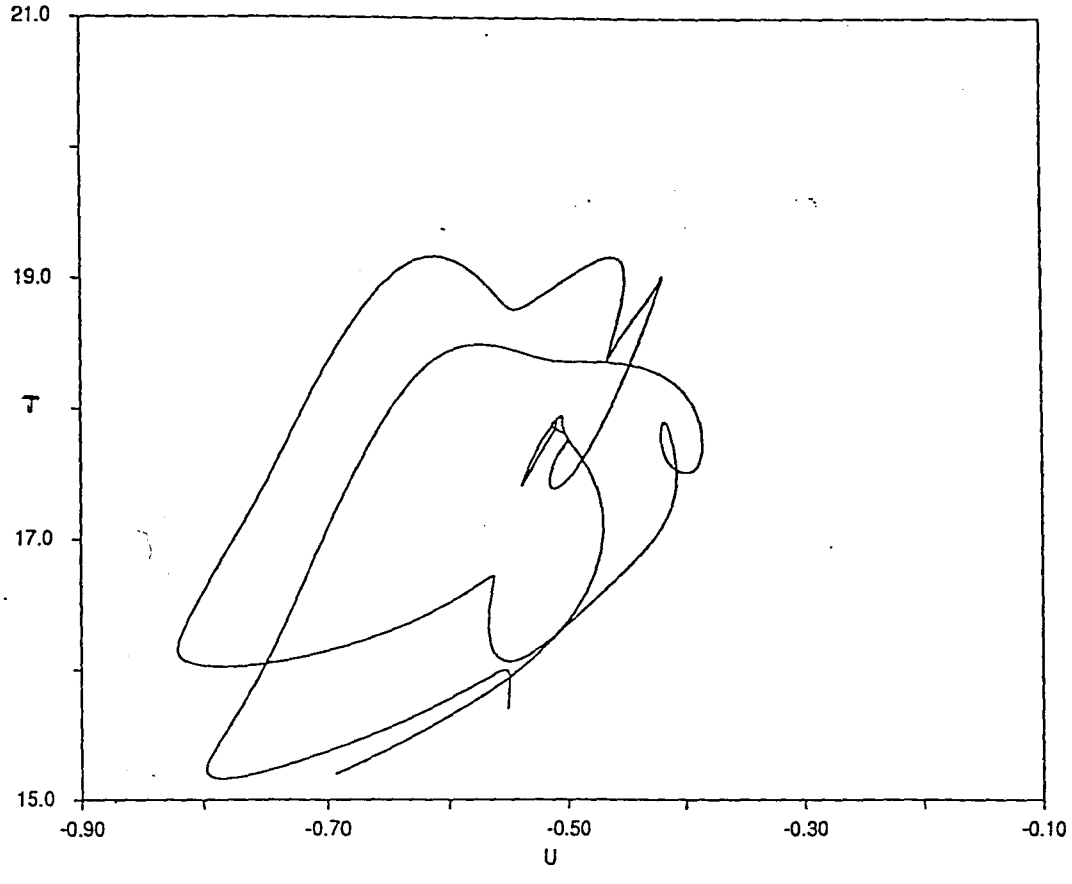

Figure 3.11 :
Phase portrait for Gr=7.5×10^5
Temperature vs x-velocity at x*=0.75, y*=0
Case 1, chaotic behavior in time

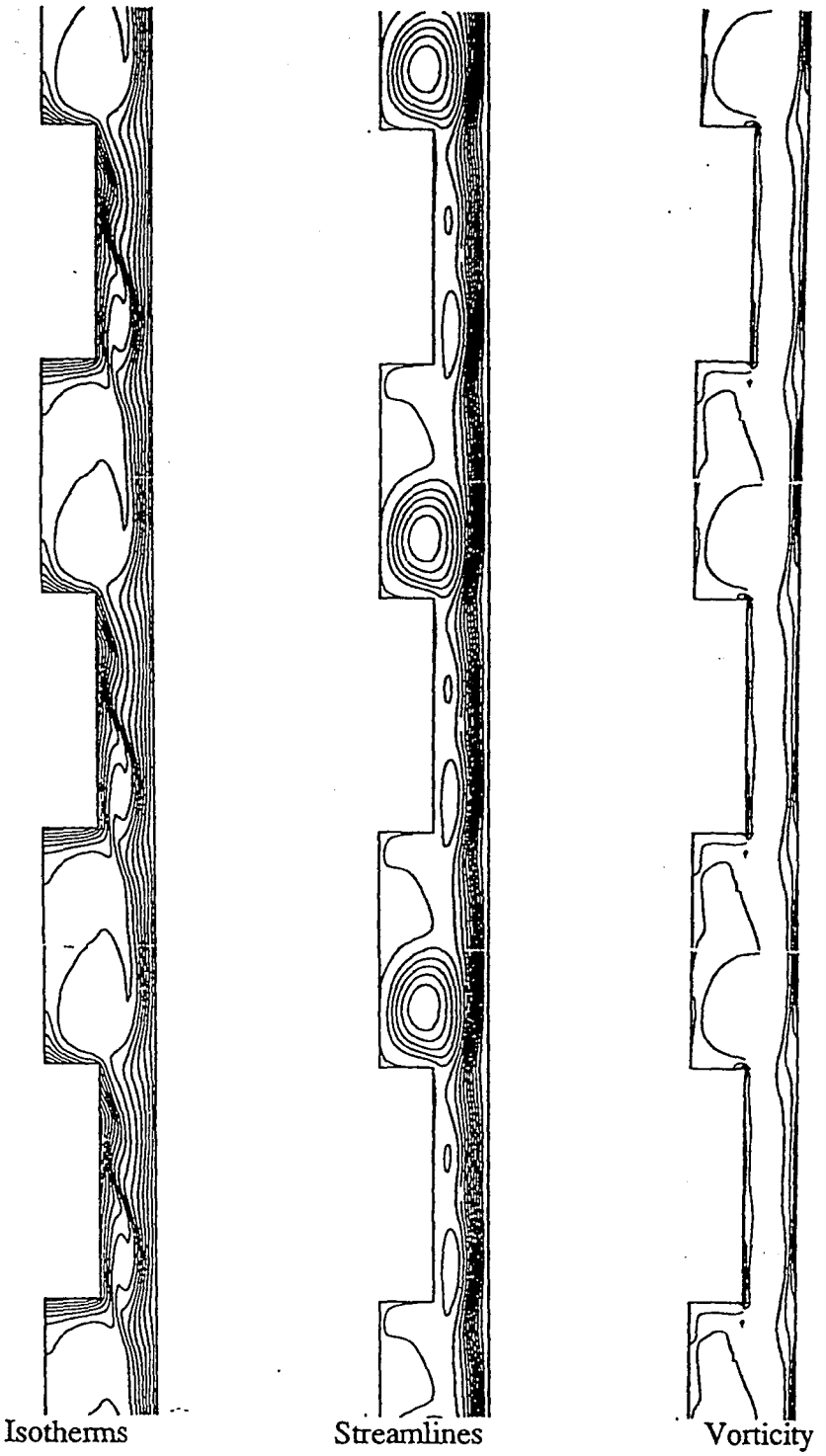

Figure 3.12:
Istantaneous isotherms, streamlines and vorticity contours
for $Gr=7.5x10^5$
Case 1, chaotic behavior in time

3.1.2 Second Case Geometry; $\frac{l_c}{l} = 3$

$$Gr \leq 1 \times 10^4$$

The results for the second case geometry exhibit the same behavior as that of the first case geometry. For low Grashof numbers, $Gr \leq 1 \times 10^4$, the maximum temperature remains the same as for the case with no flow, i.e. the conduction problem. The flows in this range of Grashof numbers are dominated by the large eddies formed in the cavities between the heating elements. Meanwhile, the flow above the heating element remains practically undisturbed. The plots of isotherms, streamlines, vorticity contours and isobars for different Grashof numbers are shown in Figures 3.13, 3.14, 3.15 and 3.16 respectively. Figure 3.17 shows changes in the local Nusselt number as the Grashof number is increased.

$$1 \times 10^4 < Gr < 1 \times 10^5$$

In this range, T^*_{max} decreases significantly as a result of the stronger flow distortions (refer to Figure 3.14). As one can see from the streamfunction plot for $Gr=1 \times 10^5$, the distortions in the flow field are caused by the formation of elongated eddies above the heating element and the elongation of eddies in the cavities between the heating elements. The increase in flow distortions can also be seen from the disturbed isotherm patterns especially in the cavities between the protruding heat sources. For this range of Grashof numbers, T^*_{max} is reduced about 40 percent relative to the conduction solution. The plot of T^*_{max} vs Grashof number is shown in Figure 3.18.

$$2 \times 10^5 < Gr \leq 4 \times 10^5$$

As Grashof number is increased to a range of 2×10^5 and 4×10^5 the steady state solutions become time-periodic as shown in phase-plane plots. Figure 3.19 shows the phase plots of temperature vs x-velocity for the respective Grashof numbers. The distortions in the flows are significantly increased and are shown in Figure 3.14. Smaller eddies are starting to form above the heat source resulting from the elongation of large eddies in the cavities. The frequencies that exist in the time periodic signals are calculated using Fast Fourier Transform (FFT). The results are depicted in Figure 3.20 and they indicate that as Grashof number is increased, the fundamental frequency is shifted to the right. In other words, the frequency of oscillation increases with Grashof number.

Figure 3.21 provides frame by frame or instantaneous plots of isotherms, streamlines, and velocity vector field within a period of oscillation for Grashof number of 4×10^5. The streamline plots show that as the cycle progresses, eddies inside the cavities elongate and form smaller eddies above the heating element. The small eddies are moving downward throughout the cycle. Figure 3.21 also shows that the amplitude of oscillation increases with Grashof numbers.

$Gr \geq 5 \times 10^5$

For Grashof number is increased above 5×10^5, the steady state solutions loose their periodicity in time. The history plots become irregular. The FFT analysis indicates that there exist a large number of frequencies in the time-history of any quantity, harmonic and sub-harmonic. The analysis using phase plots also reveals that the resulting steady state solutions are non-periodic. From both FFT analysis and phase portraits, one can conclude that the steady state solutions for $Gr \geq 5 \times 10^5$ are chaotic in time. The results of FFT analysis and phase portraits are shown in Figures 3.22 and 3.23 respectively. Plots of isotherms, streamlines and vorticity contours are presented in Figure 3.24.

One important point to note is that for both geometries, the downward non-dimensional volume flow rate (Q*) increases with Grashof number (refer to Figure 3.25) where

$$Q^* = \frac{Ql^2}{\alpha}$$

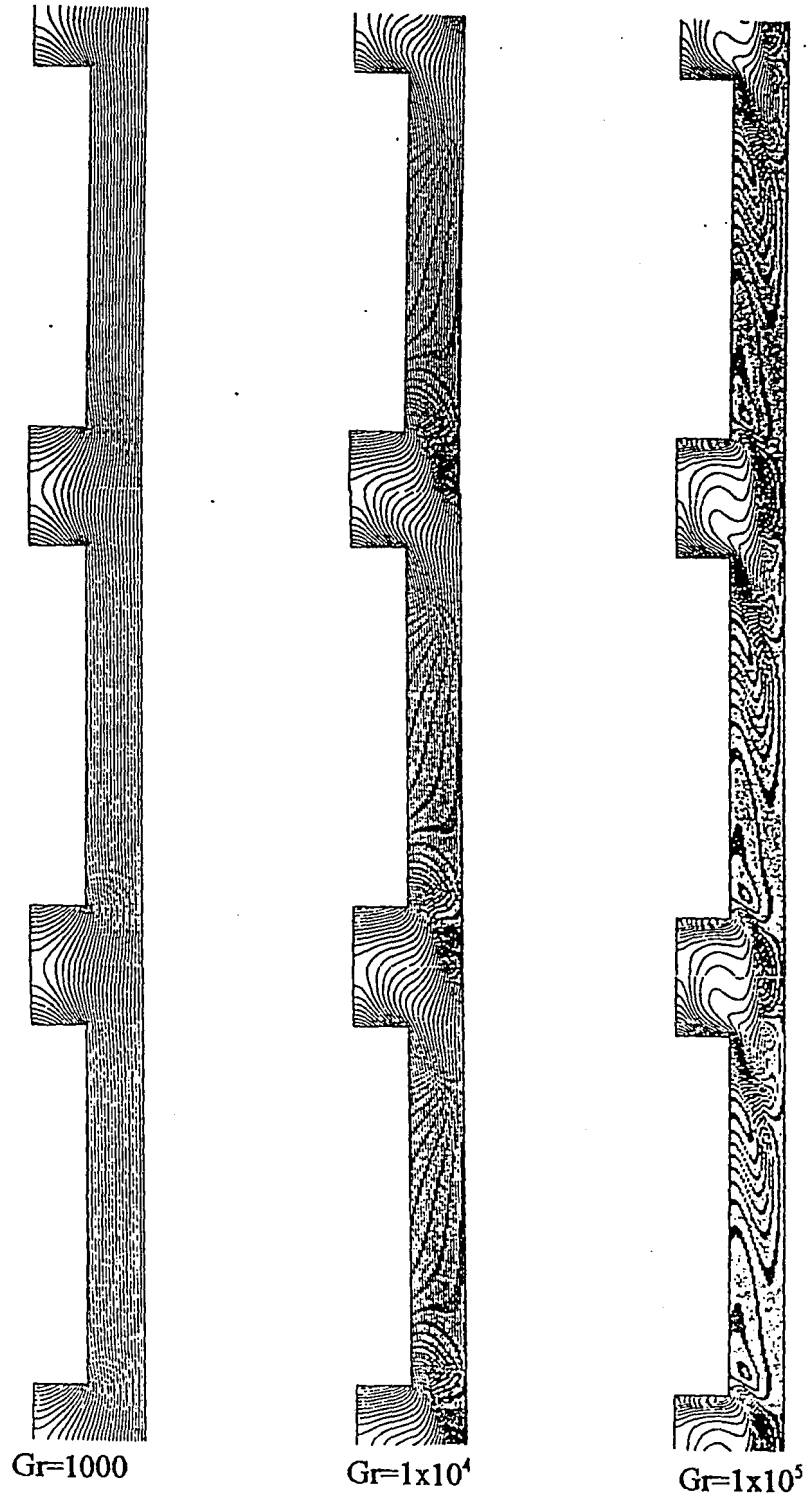

Figure 3.13 :
Isotherms for laminar flow model: case 2

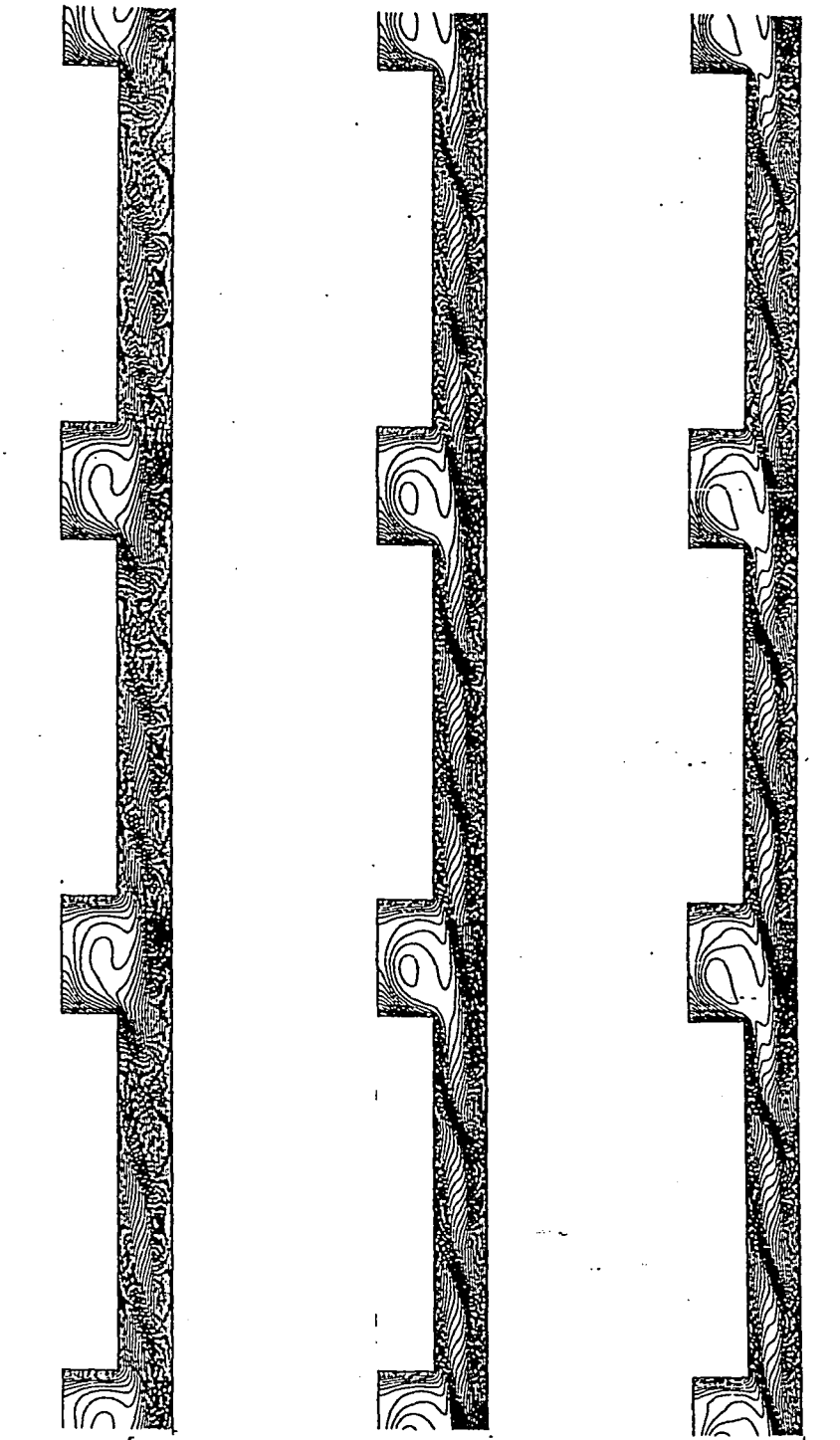

Figure 3.13(cont'd) :
Isotherms for laminar flow model : case 2

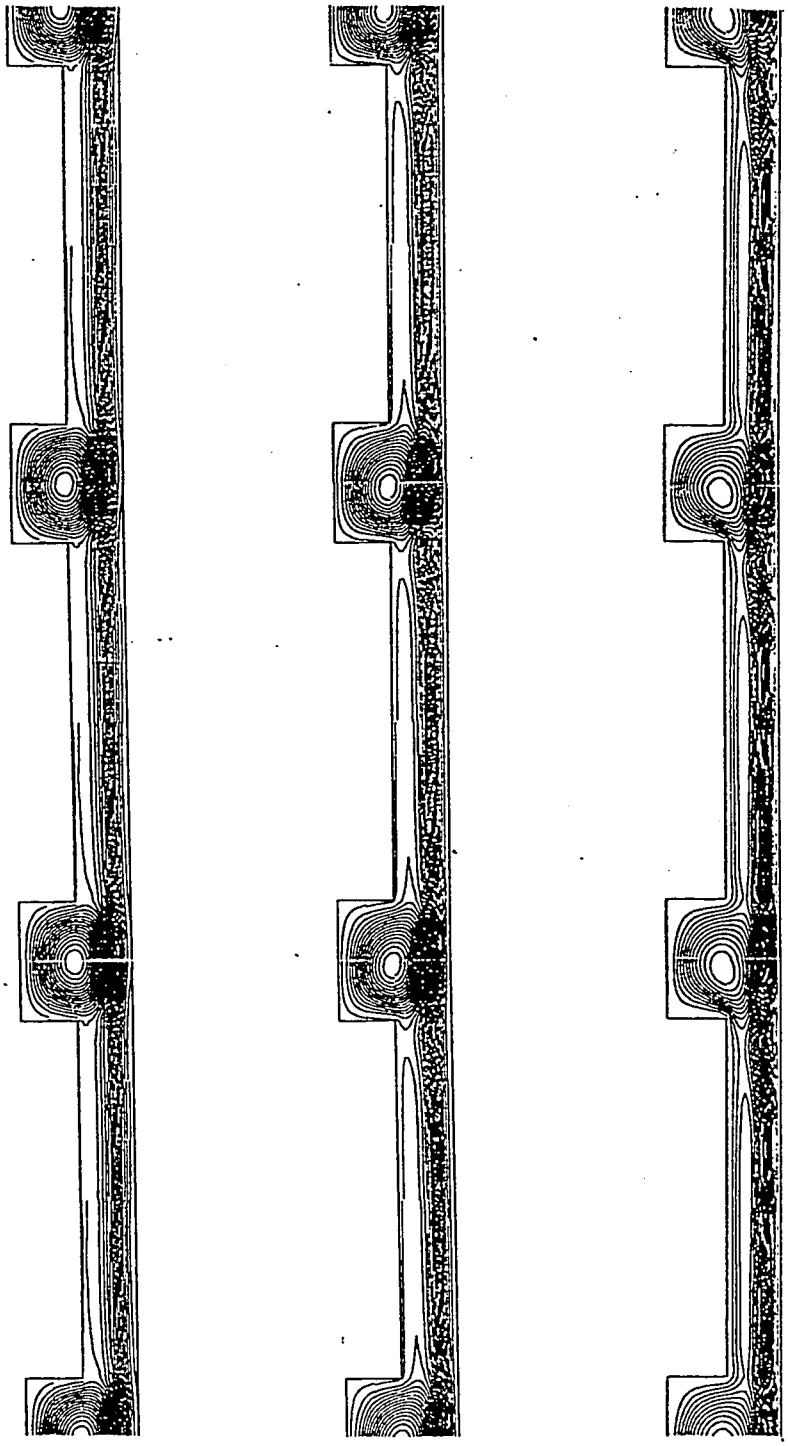

Figure 3.14 :
Streamlines for laminar flow model : case 2

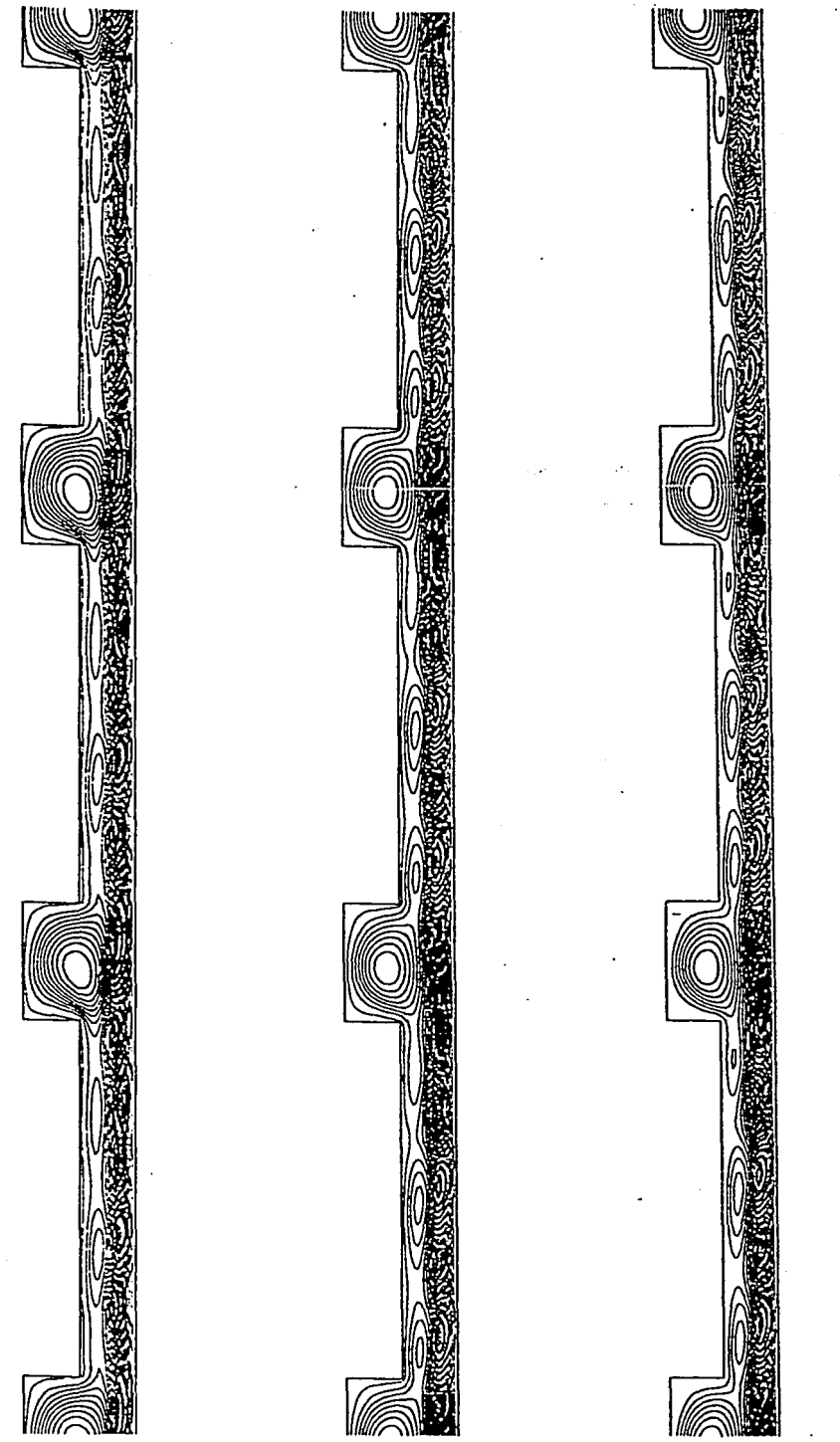

Figure 3.14(cont'd) :
Streamlines for laminar flow model : case 2

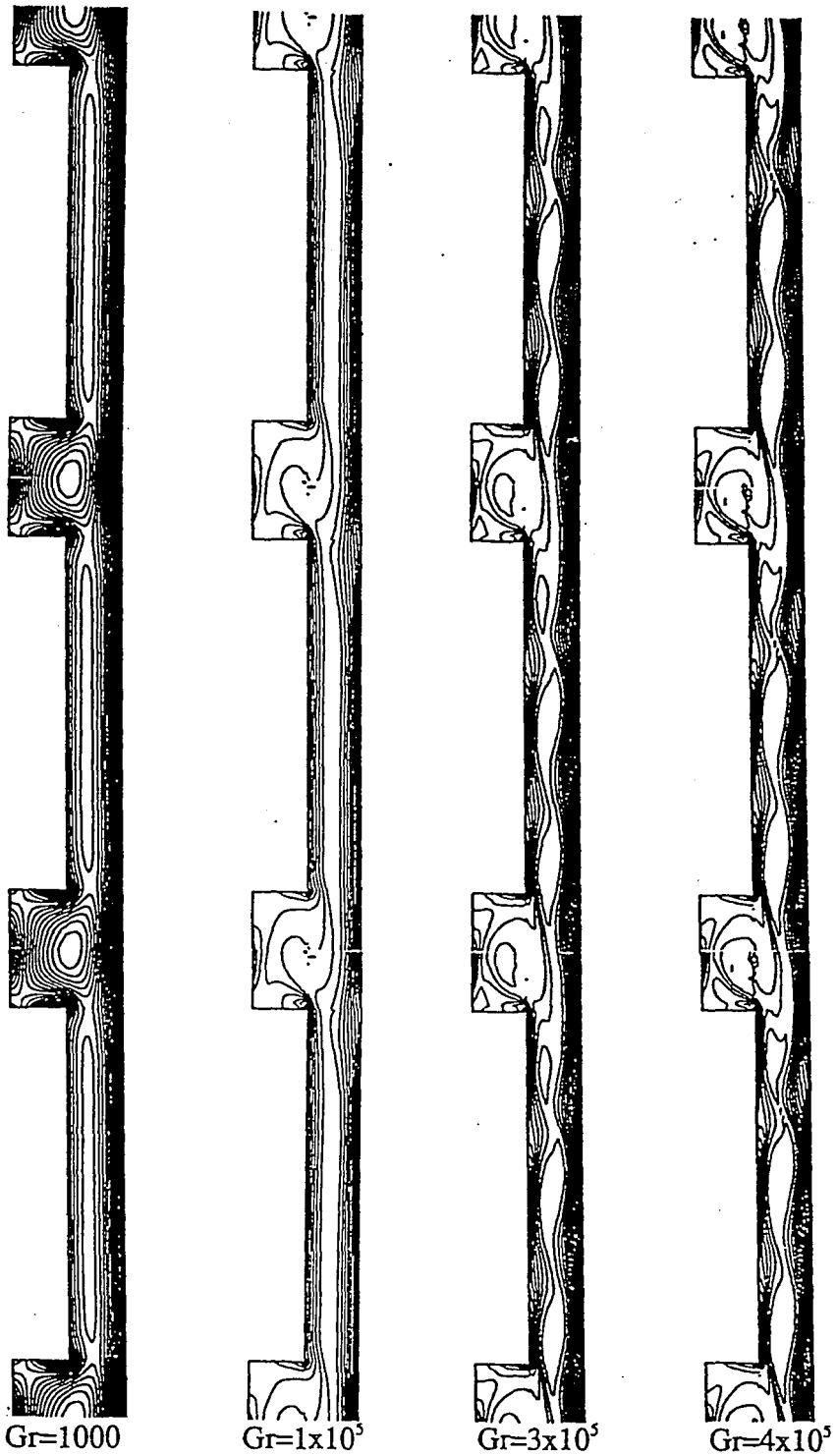

Figure 3.15 :
Vorticity contours for laminar flow model : case 2

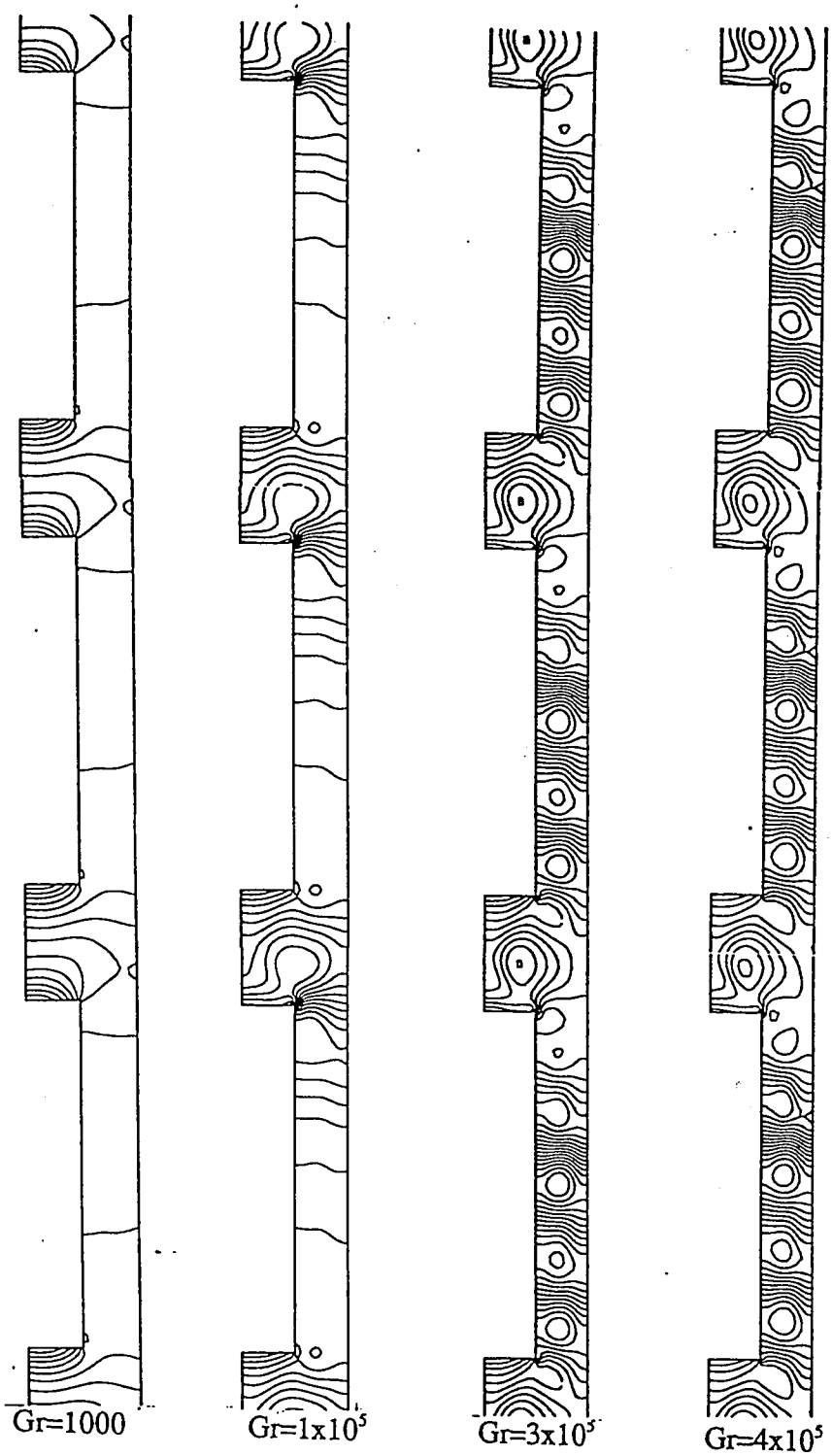

Figure 3.16 :
Isobars for laminar flow model : case 2

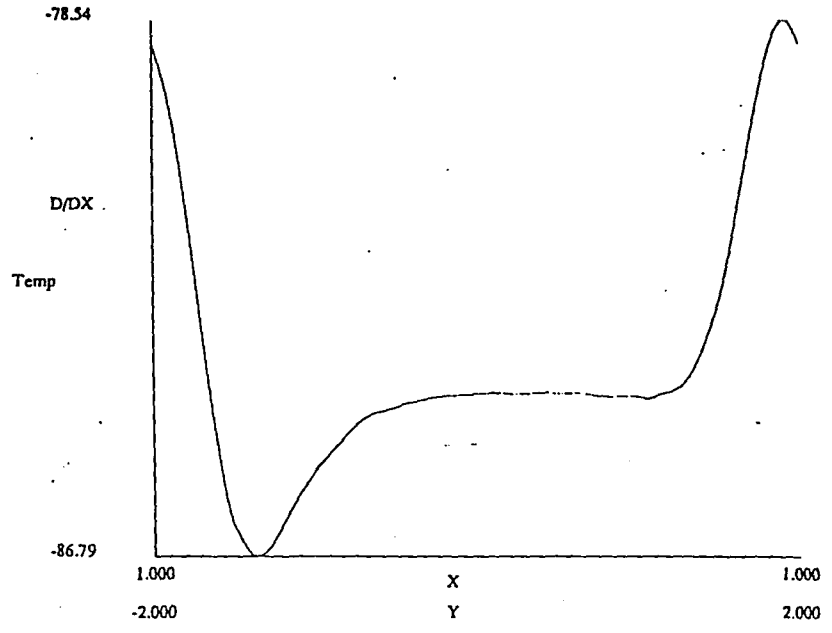

(a)

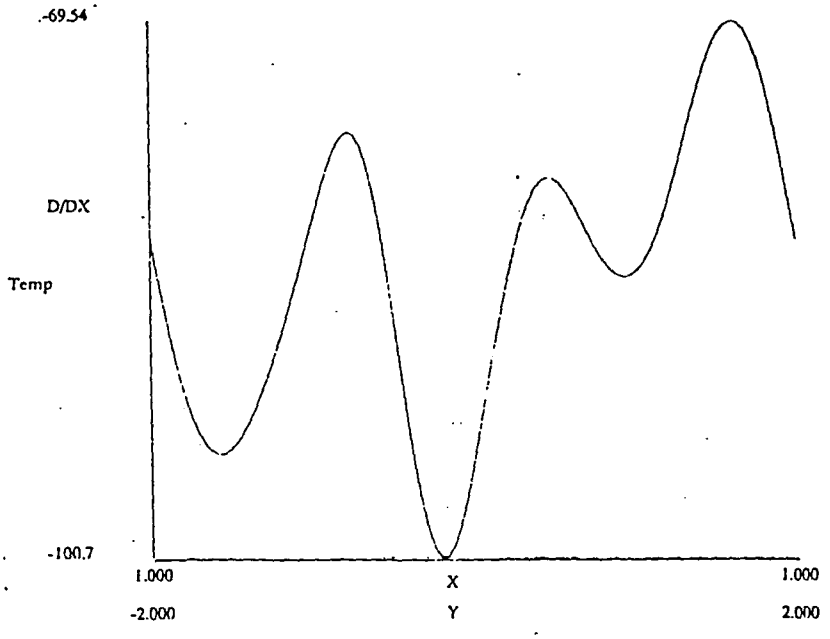

(b)

Figure 3.17:
dT/dx at x*=1 and -2<y*<2 : case 2
(a) Gr=100; (b) Gr=$2x10^5$

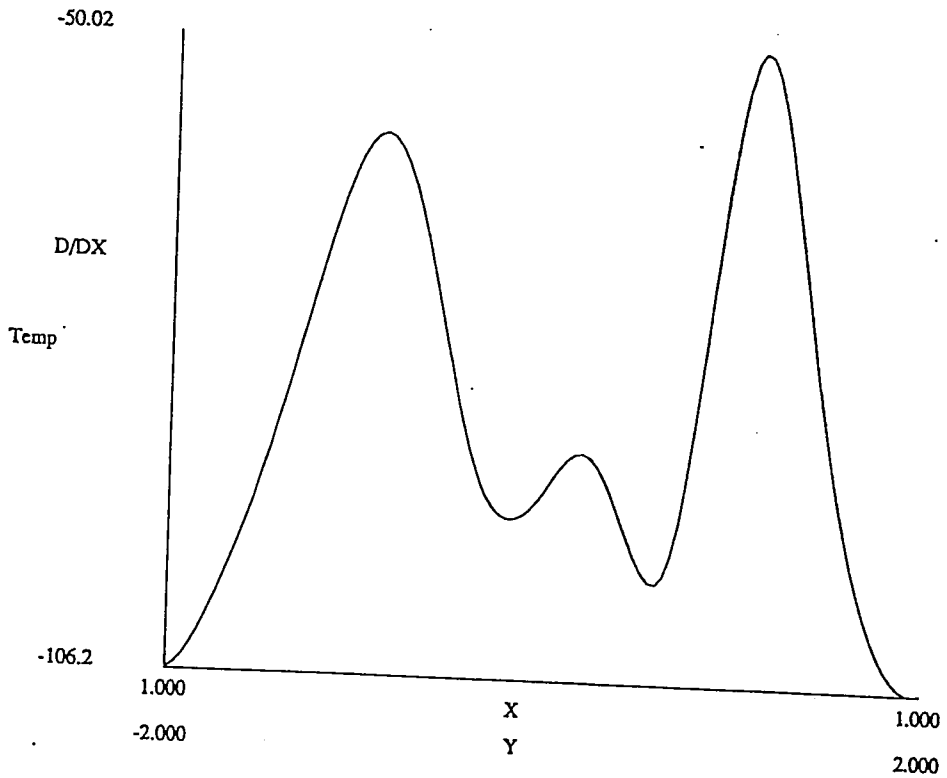

(c)

Figure 3.17 (cont'd):
$\partial T/\partial x$ at $x^*=1$ and $-2<y^*<2$: case 2
(c) $Gr=5x10^5$

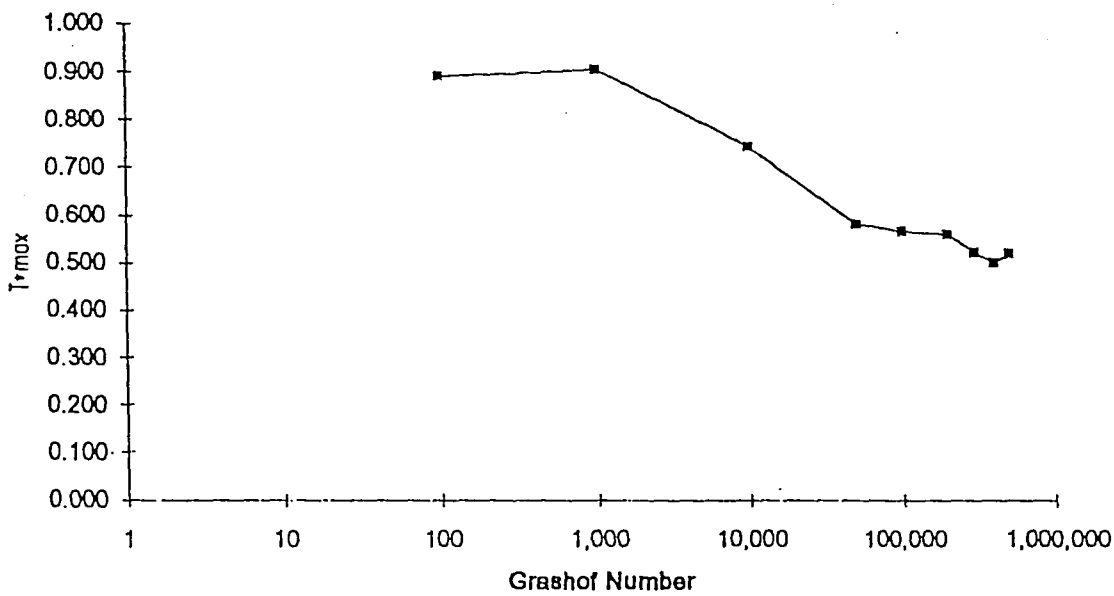

Figure 3.18 :
Dimensionless maximum temperature, T^*_{max} vs Grashof number : case 2

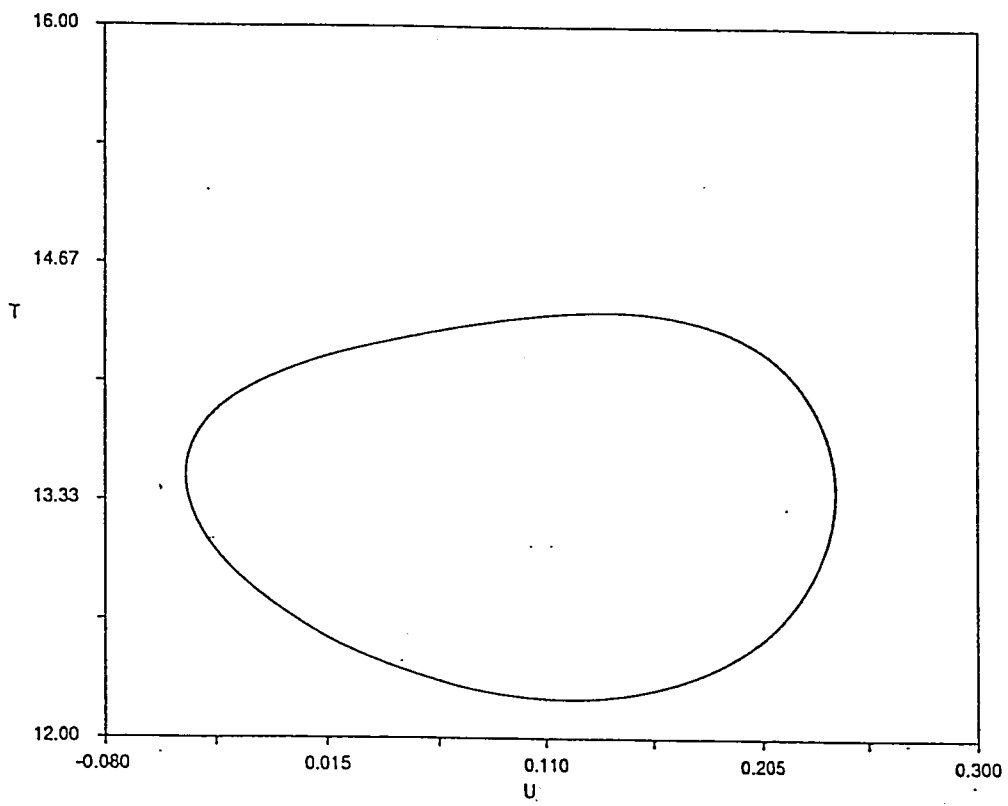

Figure 3.19 :
Phase portrait for Gr=2 x 10^5, case 2
Temperature vs x-velocity
$x^* = 0.75$, $y^* = 0$

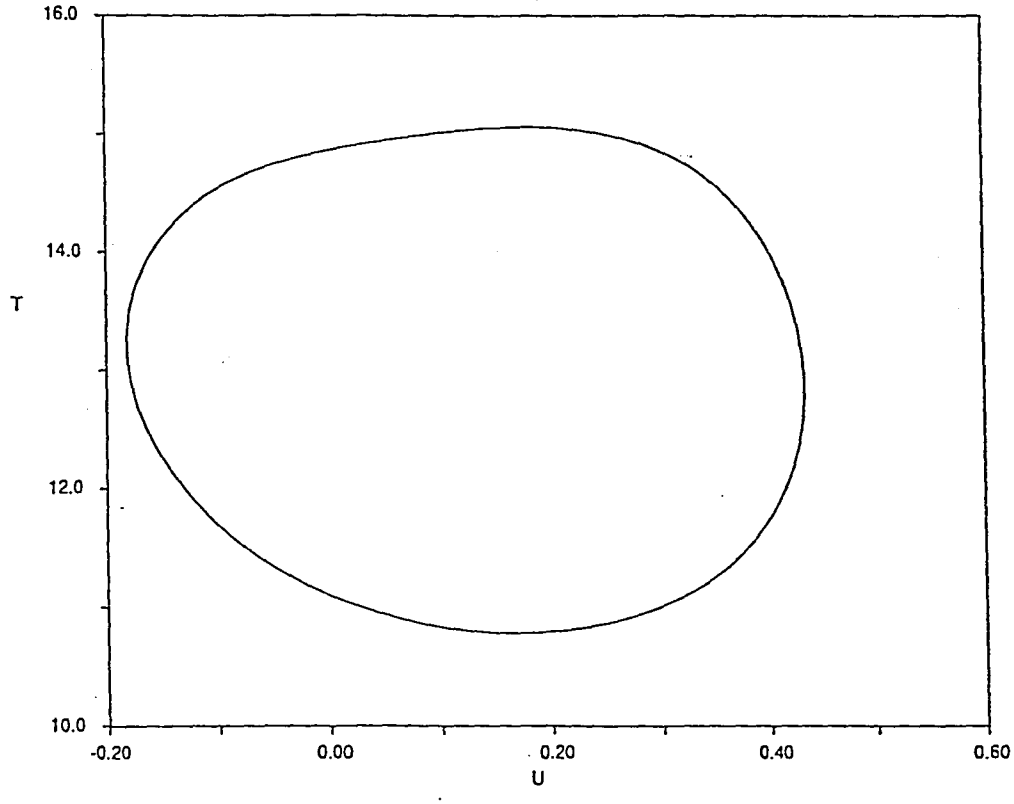

Figure 3.19(cont'd) :
Phase portrait for Gr=3 x 10^5:
Temperature vs x-velocity
x* =0.75, y* = 0

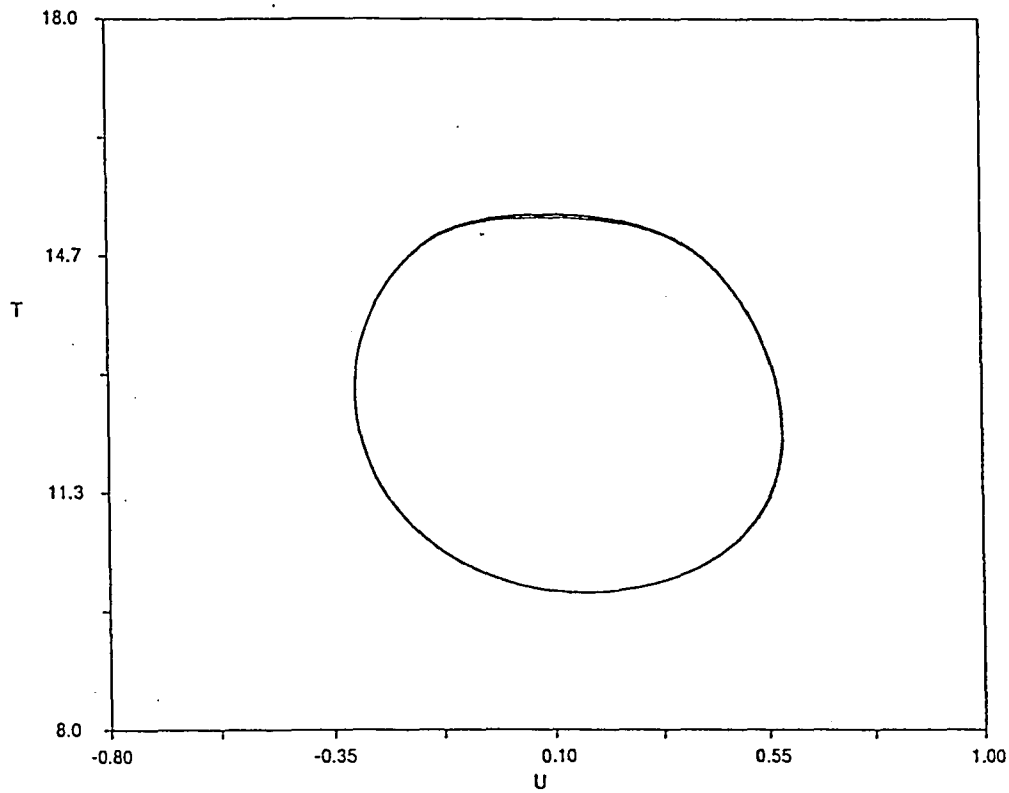

Figure 3.19(cont'd):
Phase portrait for Gr=4 x 10^5:
Temperature vs x-velocity
x* =0.75, y* =0

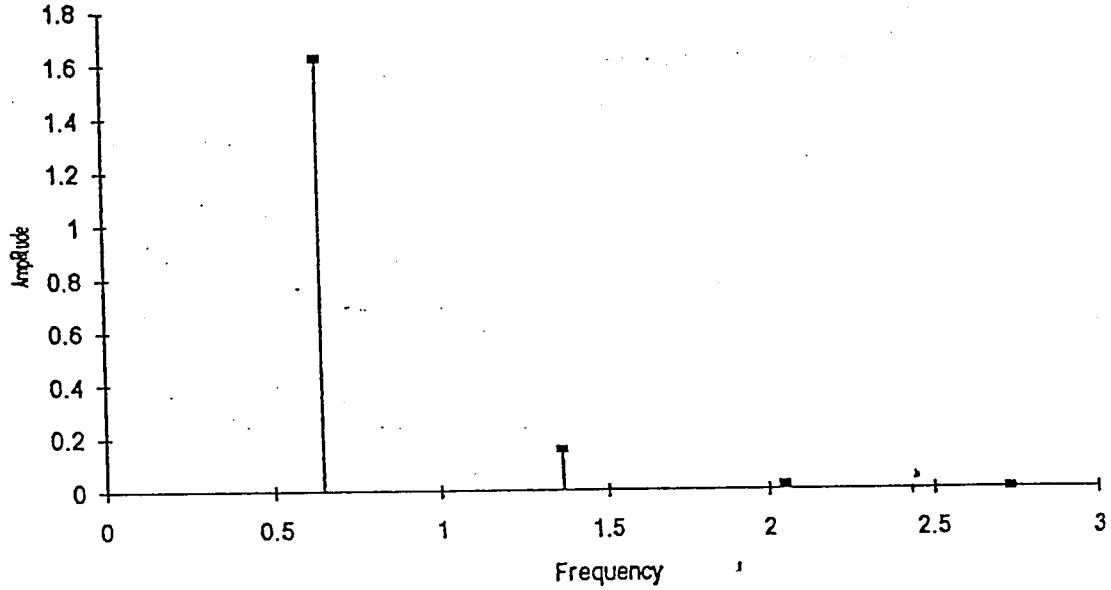

(a)

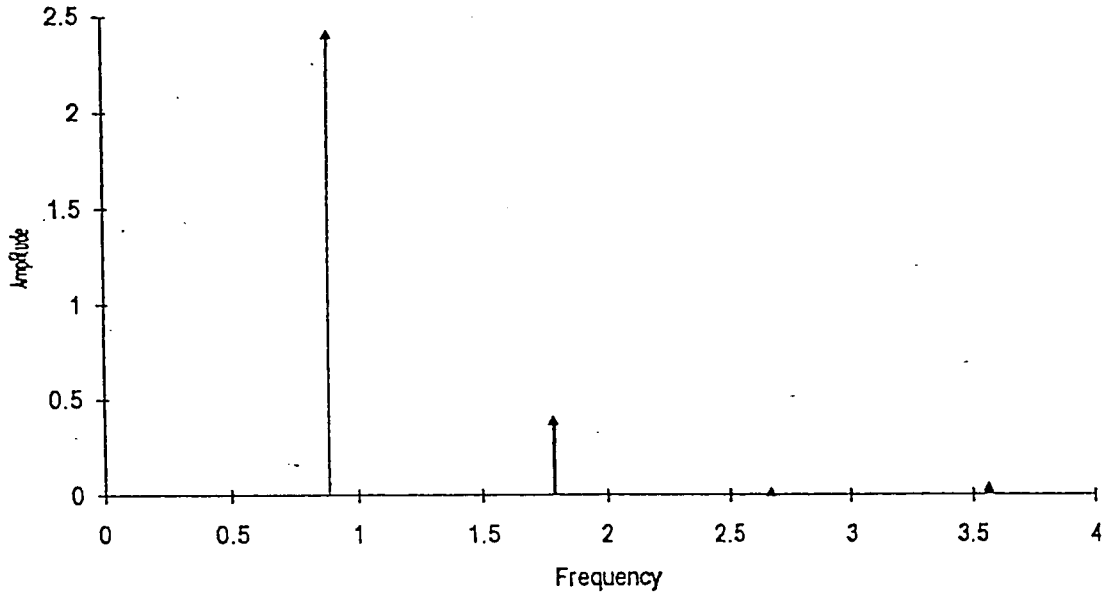

(b)

Figure 3.20:
FFT Analysis of temperature for
(a) Gr=2 x 10^5; (b) Gr=3 x 10^5
at x* =0.75, y* =0

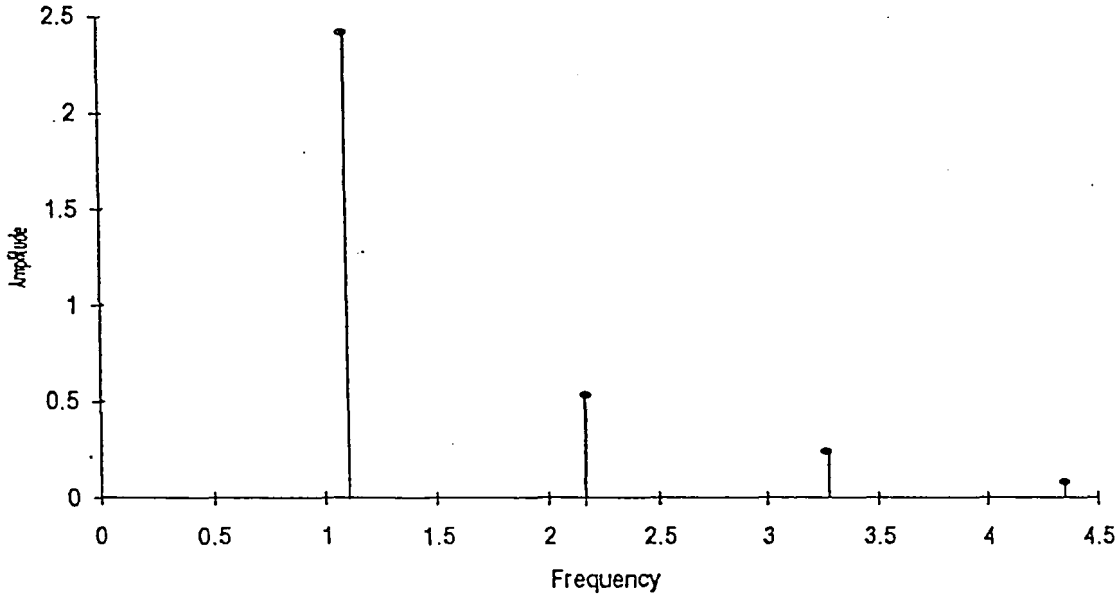

Figure 3.20(cont'd) :
FFT Analysis of temperature for
(c) $Gr=4 \times 10^5$
at $x^* = 0.75$, $y^* = 0$

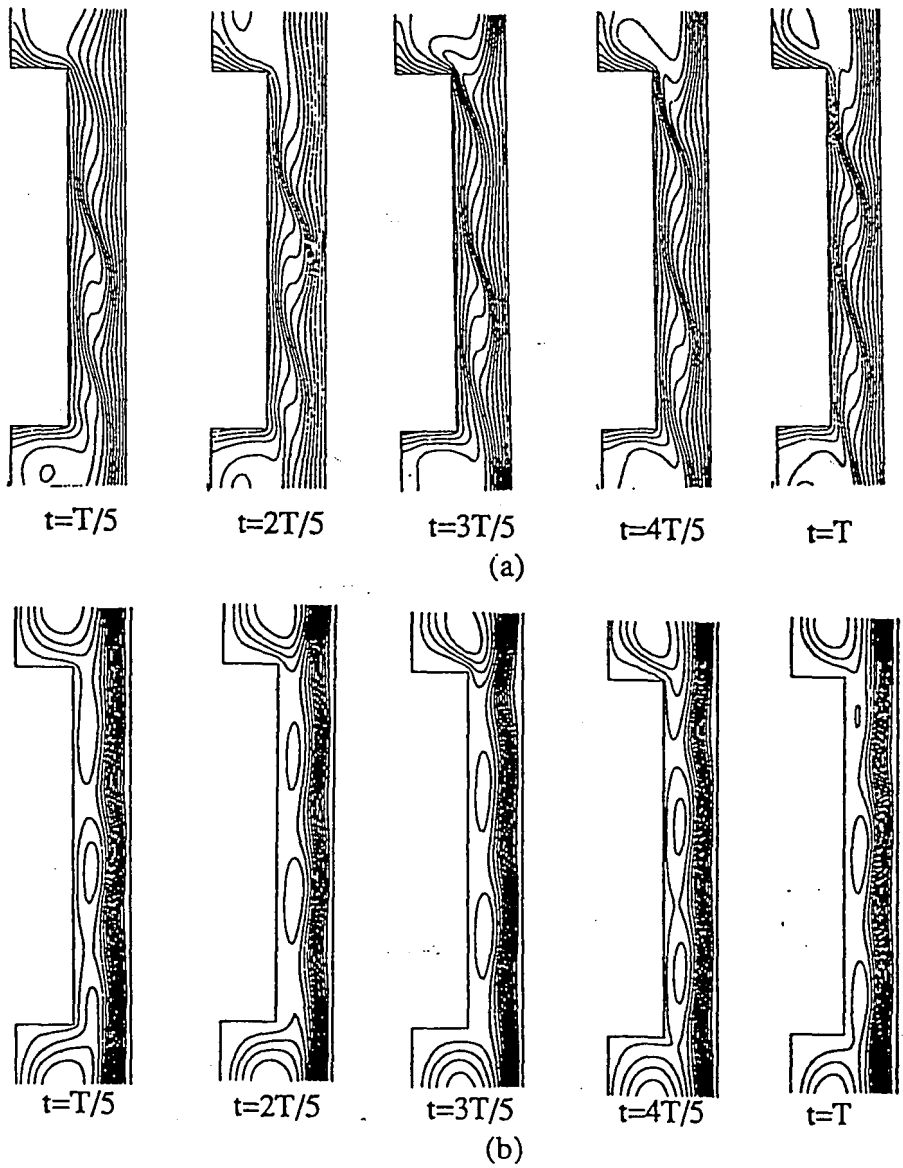

Figure 3.21 :
Plots for Instantaneous
(a) Isotherms; (b) Streamlines
$Gr=4x10^5$

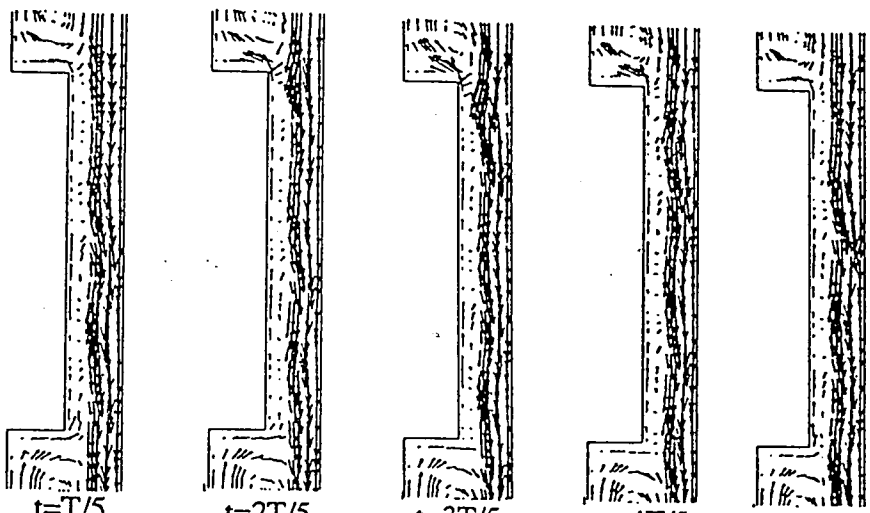

(c)

Figure 3.21 (cont'd) :
Instantaneous
(c) velocity vectors
$Gr=4x10^5$

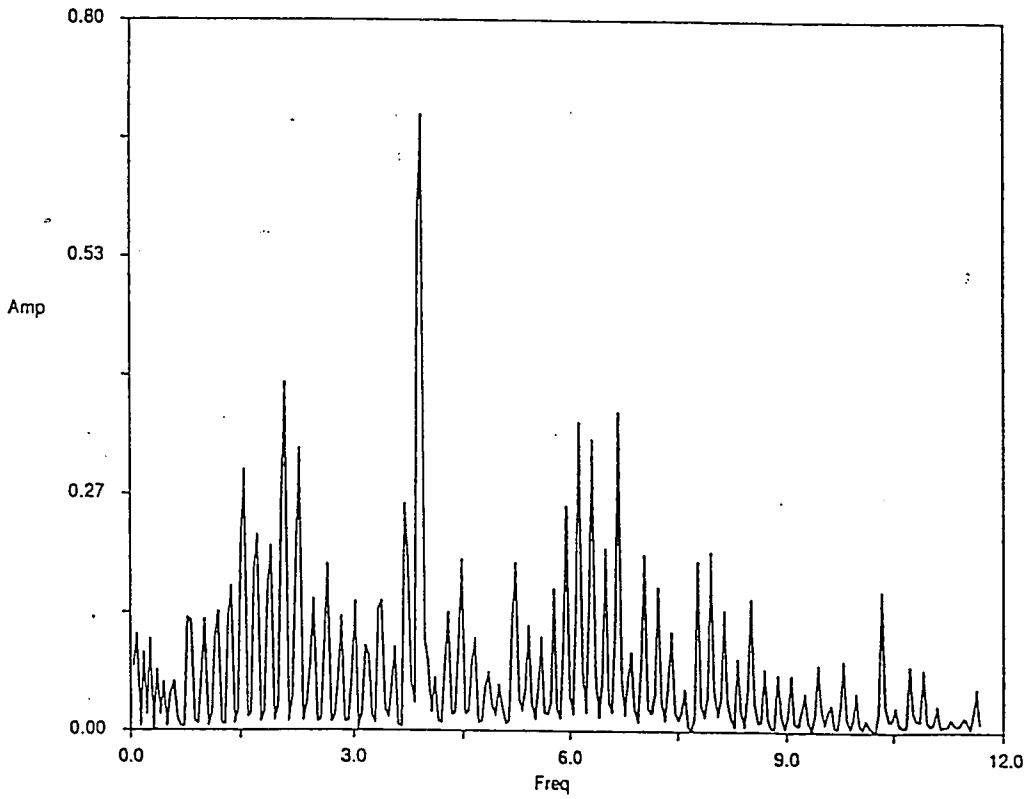

Figure 3.22 :
FFT analysis of pressure for Gr=$5x10^5$ at x* = 0.75, y* =0
Case 2, chaotic behavior in time

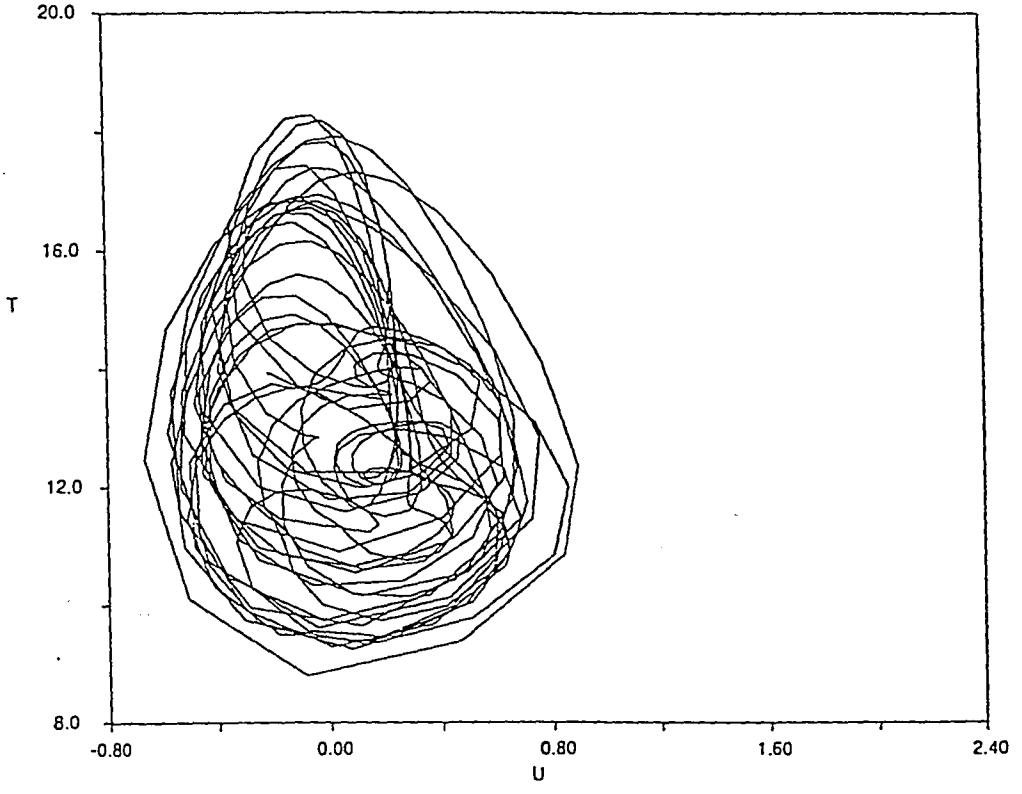

Figure 3.23:
Phase portrait for $Gr=5x10^5$ at $x^*=0.75$, $y^*=0$
Case 2, chaotic behavior in time

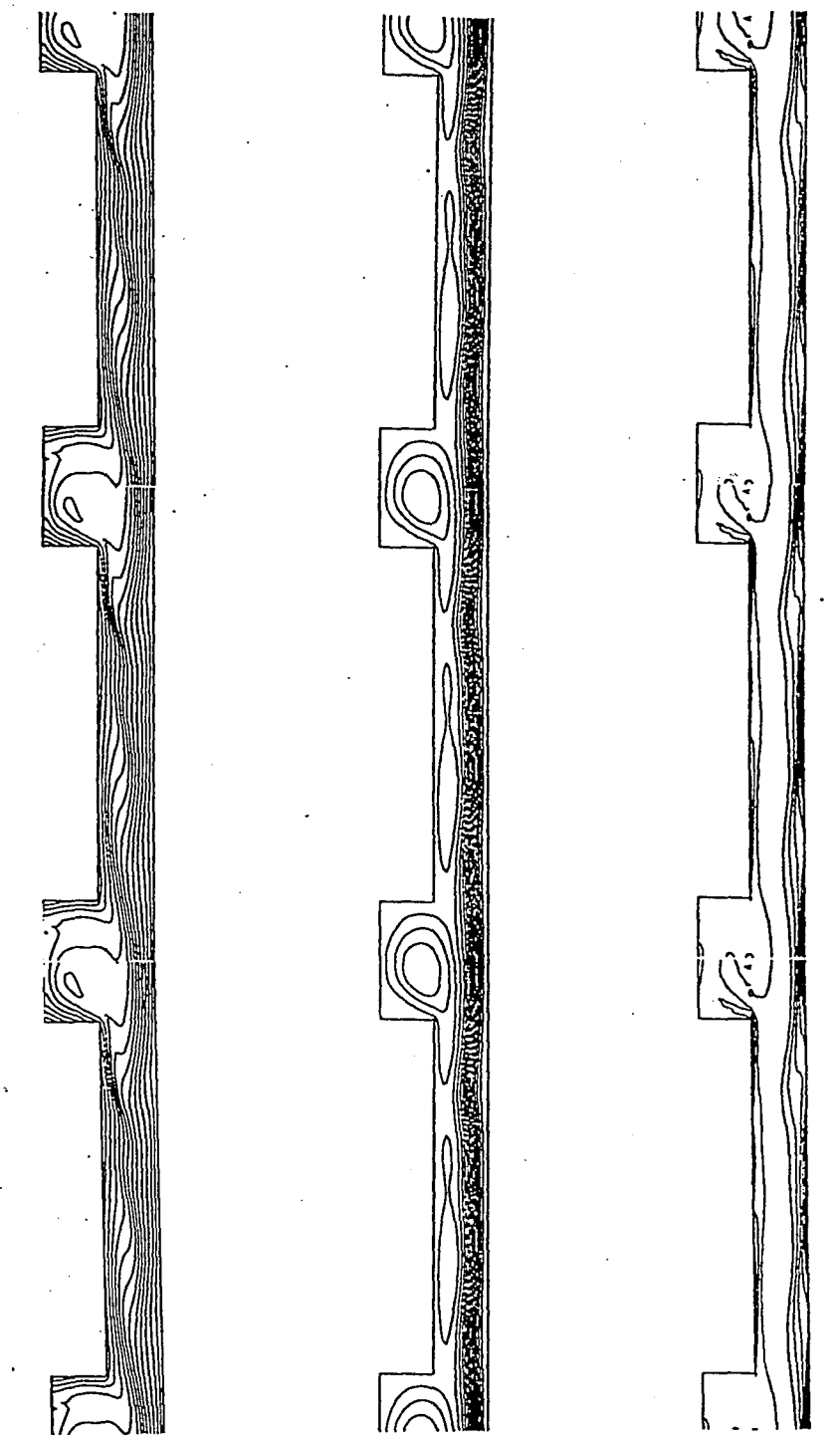

Figure 3.24 :
Instantaneous isotherms, streamlines and vorticity contours
for $Gr=5x10^5$
Case 2, chaotic behavior in time

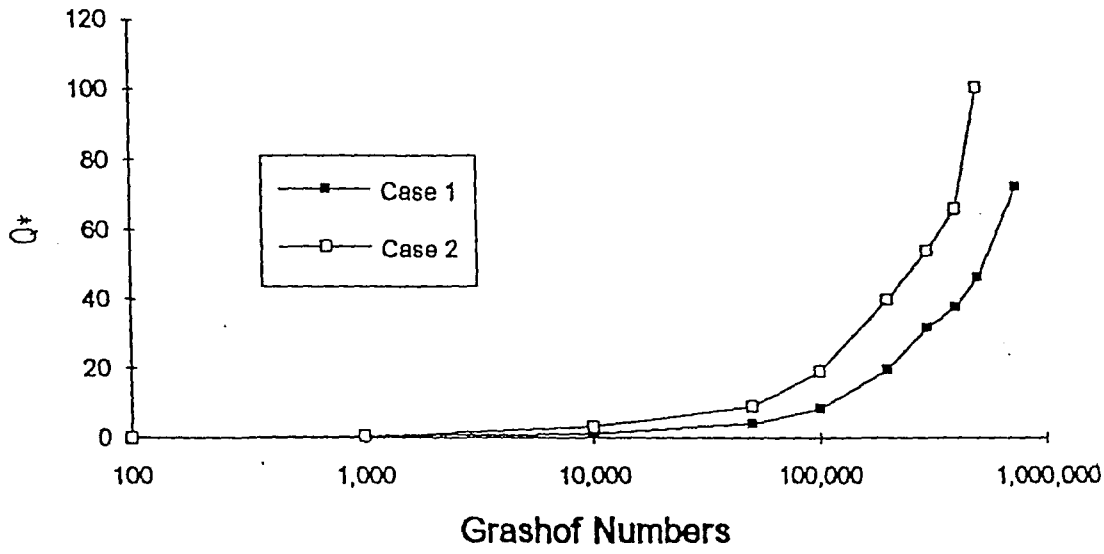

Figure 3.25 :
Dimensionless net volume flow rate Q* vs Grashof number
for cases 1 and 2

3.2 Turbulent Flow

The turbulent flow calculations were based on the mixing length assumption. Because of the unavailability of experimental data on the mixing length for the flow studied, the author used the default value of 0 .14 for the mixing length - which is based on experiments with flows in a pipe. Because the turbulent flow occurs at high Grashof numbers, the transient period (the period before reaching steady state) is too long if the calculation is started using the solution for Gr = 0 as initial condition. In order to avoid such long calculation, a "turbulent" flow solution for Gr=5 x 10^5 has been calculated using a laminar flow solution as the initial condition. The actual Grashof number for transition to turbulence is unknown. The presented results have not yet been experimentally tested and they are not intended for practical use before validation. The author hopes that the results will be used as a starting point for future work.

Even though the turbulent flow model was solved for both configurations, $\frac{l_c}{l} = 2$ and $\frac{l_c}{l} = 3$ only results from the first case are presented. Figures 3.26, 3.27, and 3.28 depict the isotherms, streamlines and isobars, respectively, for selected Grashof numbers; from Gr=7.5 x 10^5 to Gr=1.5 x 10^6. The isotherms and streamlines remain almost unchanged as the Grashof number is increased from 5 x 10^5 to 1 x 10^6. The isotherm pattern starts to change at Grashof numbers larger than 1.25 x 10^6. For $Gr < 1.25 \times 10^6$, the temperature decreases with increasing Grashof number. However, for $Gr > 1.25 \times 10^6$, the maximum temperature comes back up (as shown in Figure 3.29). Accordingly, the critical Grashof number for transition to turbulence is 1.25 x 10^6.

However, it should be noted that this is a conjecture at this point and has to be verified experimentally. Similar behavior can also be observed in the streamline plots, as the Grashof number is increased. From the streamline plots, one can see that the flow is mostly dominated by a large eddies formed in the cavity between the heating elements. A smaller eddies can also be observed above the heating element. The streamline plots of time-averaged flow do not indicate any abrupt changes in the flow field as the critical Grashof number is encountered.

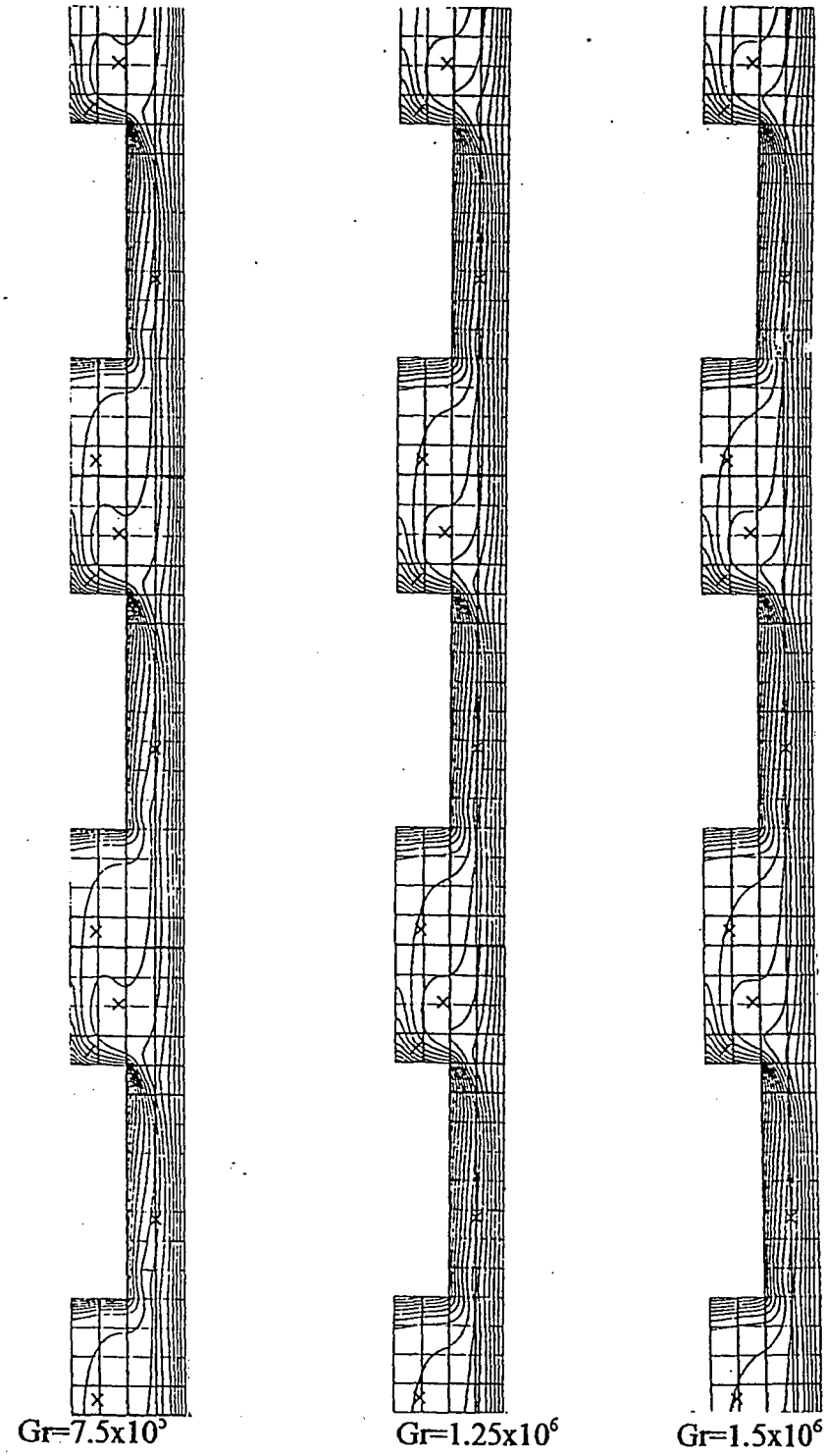

Figure 3.26 :
Isotherms for turbulent flow

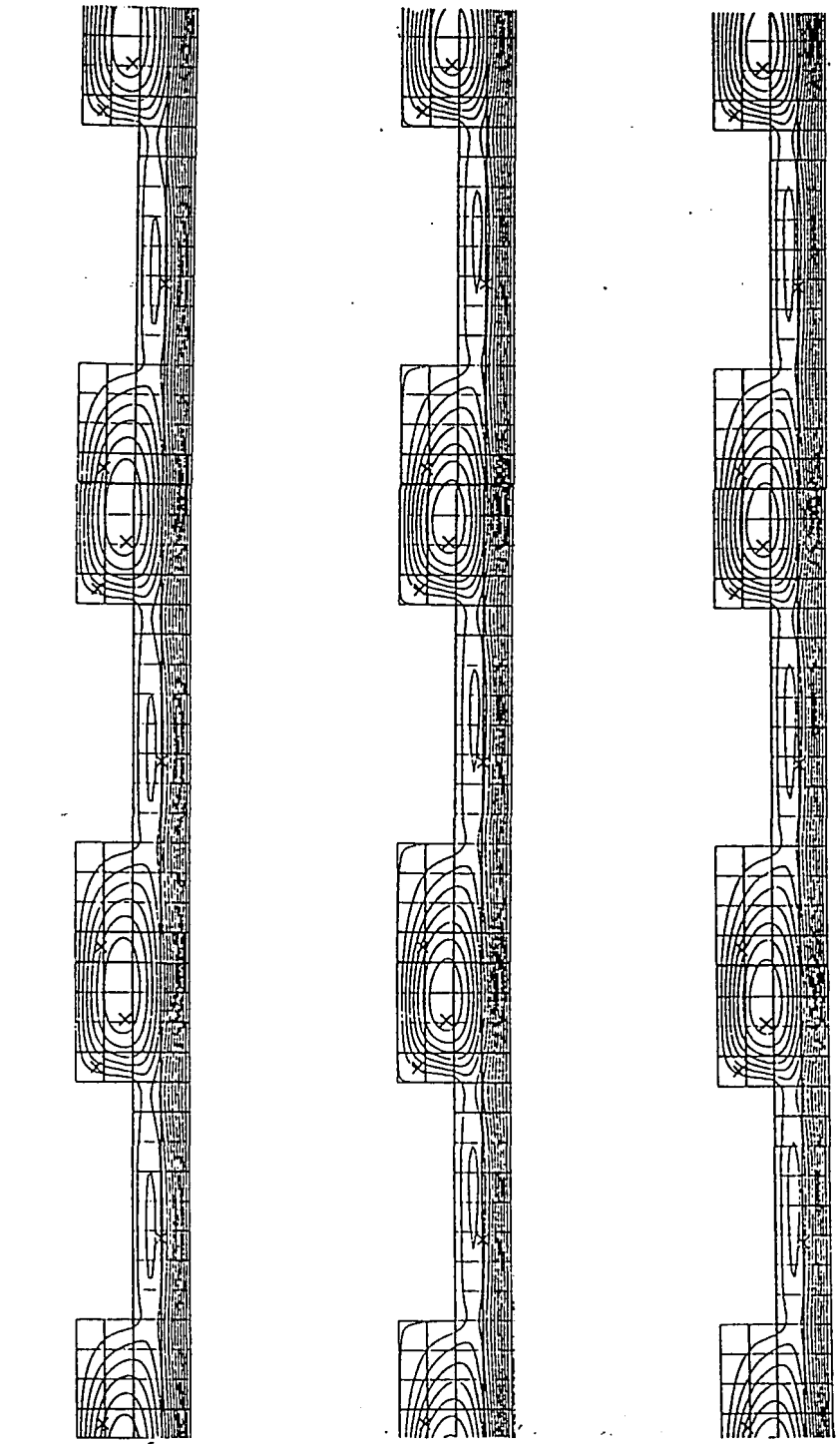

Figure 3.27 :
Streamlines for turbulent flow

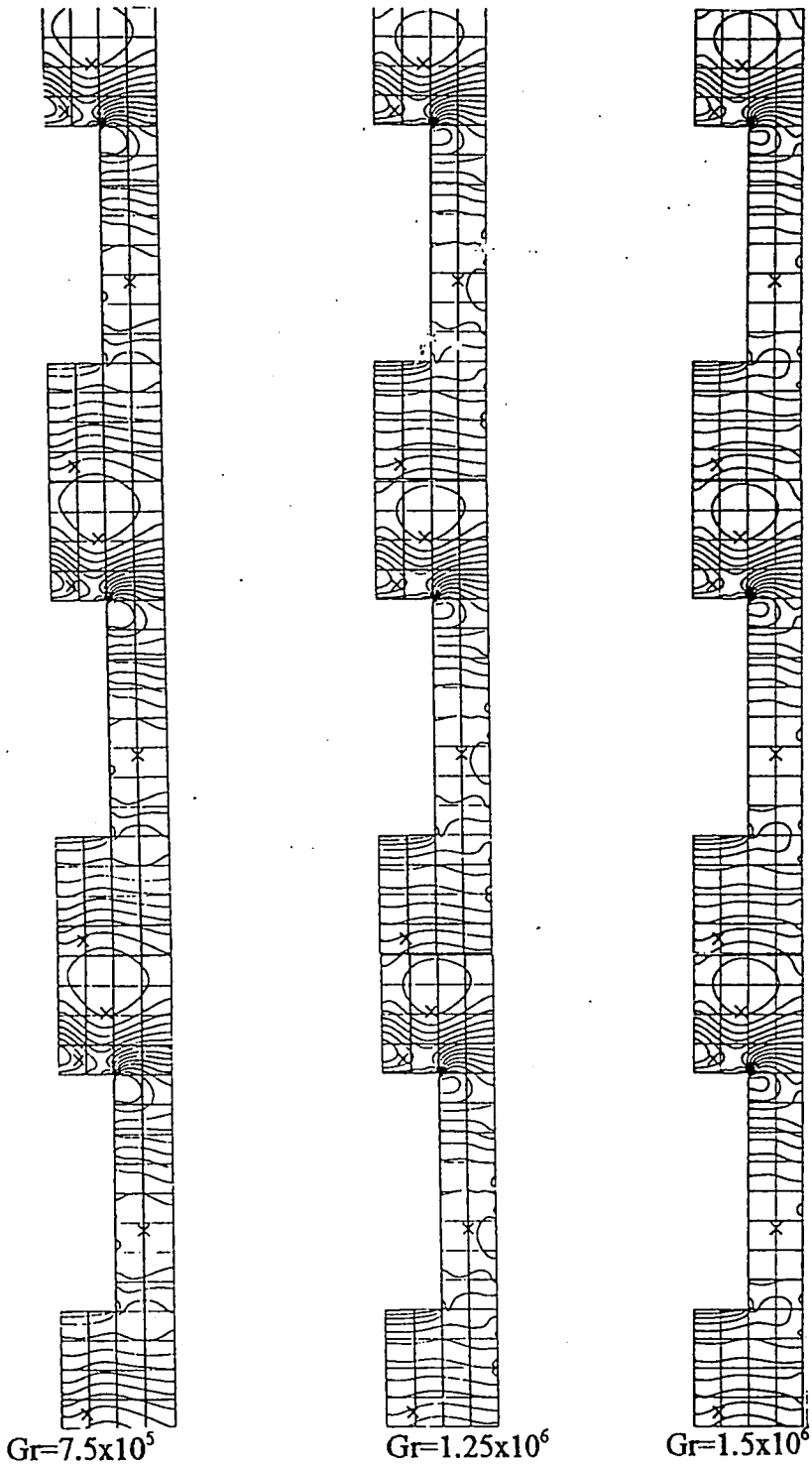

Figure 3.28 :
Isobars for turbulent flow

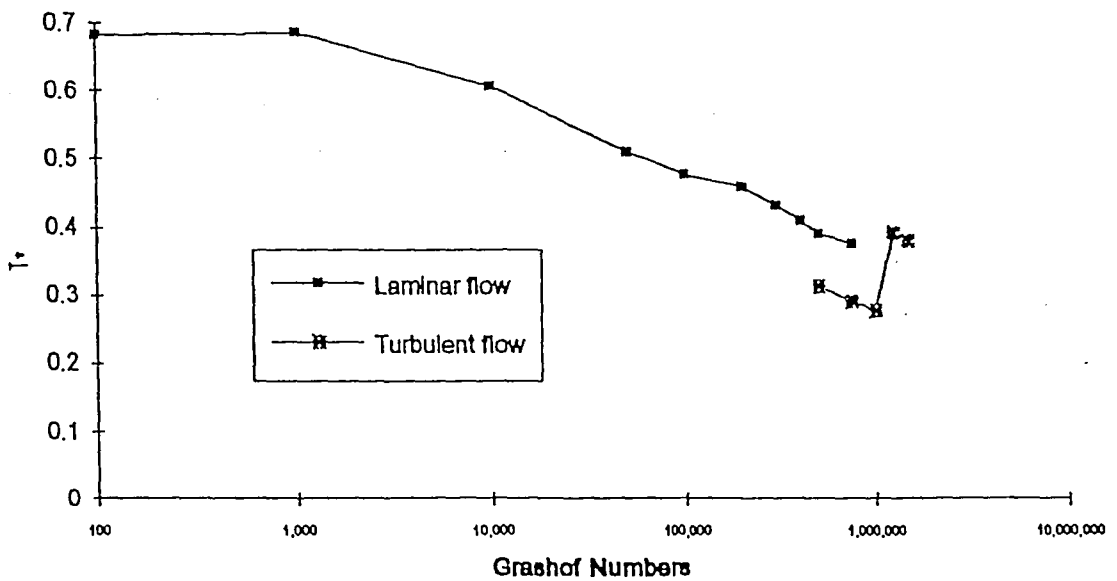

Figure 3.29:
Dimensionless maximum temperature, T^*_{max} vs Grashof number
for laminar and turbulent flows

3.3 Sample calculations for typical air-filled cavities encountered in second level packaging

The numerical studies in this work are intended to provide guidelines in designing natural convection cooling systems with air as the cooling medium. From the computational point of view, the most convenient way to conduct the study for different Grashof numbers is by changing the values of βg. Thus, the study has been conducted by using a 'fictitious' fluid rather than air. The properties of the fictitious fluid are chosen so that the Pr=0.71 and the Grashof number was increased by simply increasing βg. In order to use the results presented in this study in predicting the maximum temperature in air-filled cavities, some adjustments have to be made. In practice βg is approximately constant and the Grashof number changes by changing the value of either l or the heat flux. By keeping l constant, the applied surface heat flux can be calculated for a given Grashof number. The results presented below are for values of l typical for electronic equipment.

Properties of air :

$k = 27.8 \times 10^{-3}$ W/m-K $\qquad \rho = 1.0932$ kg/m^3

$\beta = 3.12 \times 10^{-3}$ K^{-1} $\qquad \nu = 17.95 \times 10^{-6}$ m^2/s

$c_p = 1.008$ kJ/kg-K $\qquad \alpha = 25.3 \times 10^{-6}$ m^2/s

Properties of 'fictitious' fluid :

$k = .011868$ W/m-K $\qquad \rho = 1.0$ kg/m^3

$\nu = .008426$ m^2/s $\qquad c_p = 1.0$ kJ/kg-K

β = variable

Assumptions:

- The reference temperature, $T_r = 25\ ^0C$

	First case	Second case
◆	l = .035 m, .045 m	l = .035 m, .045 m
◆	l_c = .07m, .090 m	l_c = .105 m, .135 m
◆	$l_s/2$ = .035 m, .045 m	$l_s/2$ = .0175 m, .0225 m
◆	h_c = .0175 m, .0225 m	h_c = .0175 m, .0225 m

We know that for physical similarity,

$$(\frac{l_s}{l})_{model} = (\frac{l_s}{l})_{Air}$$

$$(\frac{l_c}{l})_{model} = (\frac{l_c}{l})_{air}$$

Pr: $$(\frac{\nu}{\alpha})_{model} = (\frac{\nu}{\alpha})_{air} \qquad (3.2)$$

$$\text{Gr}: \qquad \left(\frac{\beta g q'' l^4}{\nu^2 k}\right)_{\text{Model}} = \left(\frac{\beta g q'' l^4}{\nu^2 k}\right)_{air} \qquad (3.3)$$

Equation (3.2) is satisfied by the values of properties selected for the fictitious fluid used in the computational model.

The numerical study based on the properties of the fictitious fluid yielded $T^*_{max} = f(Gr\ ;\ Pr=0.71)$ as depicted in Figures 3.6 and 3.16 for both geometry cases, and the maximum temperature anticipated in air-filled cavities can be calculated using

$$T_{max_{air}} = \left(\frac{q'' l}{k}\right)_{air} \times T^*_{max} + T_r$$

The heat flux, q", can be calculated for a given l, and is used to deduce $T_{max,air}$. Figures 3.30 and 3.31 are the plots for the maximum air temperature, $T_{max,air}$ vs the heat flux, q" for different values of l for both geometric configurations.

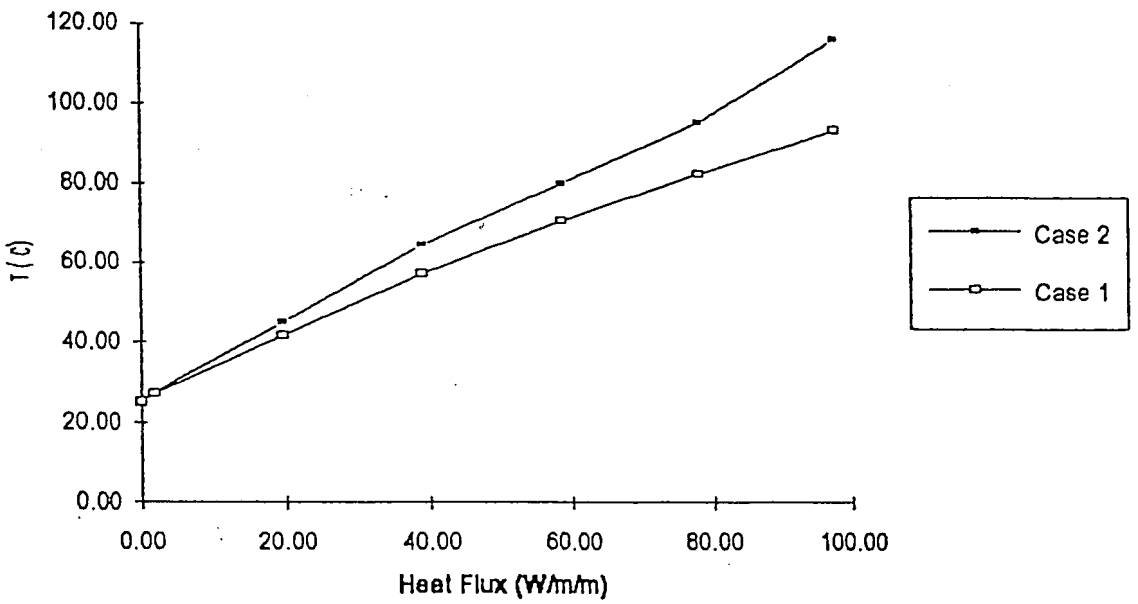

Figure 3.30:
$T_{max,air}$ vs Heat flux for l=.035m
case 1 and case 2

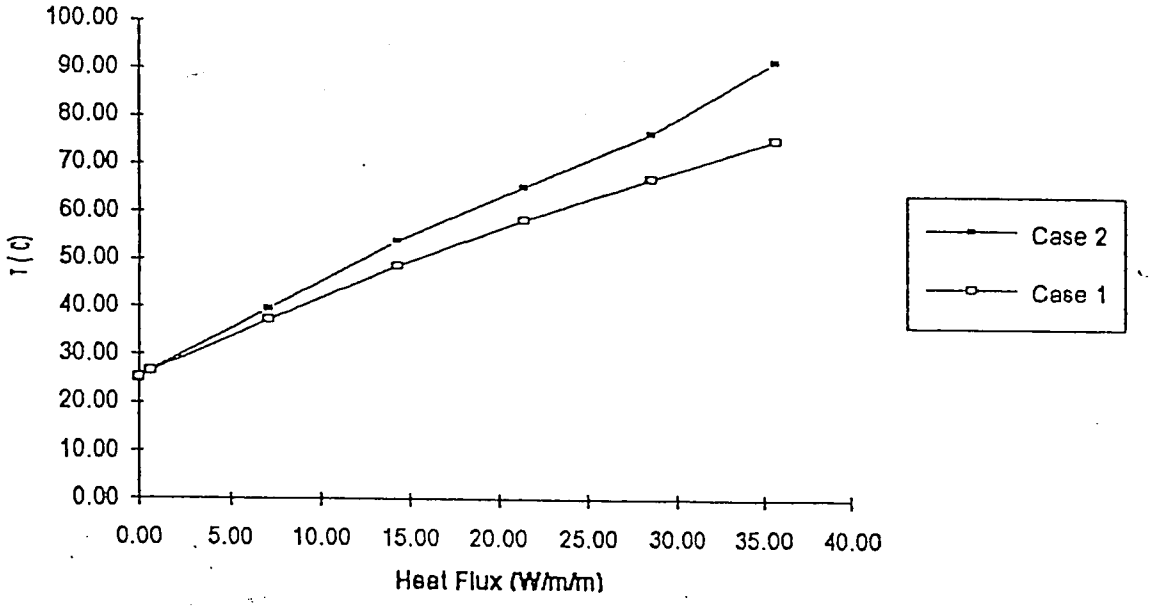

Figure 3.31:
$T_{max,air}$ vs Heat flux for l=.045 m
case 1 and case 2

CHAPTER FOUR

Conclusions & Recommendations

This study has revealed the importance of effective thermal management in improving the reliability of electronic equipment. As long as the heat fluxes remain low enough, natural convection is the most reliable and economical cooling method. The maximum temperature within electronic equipment can be effectively controlled by adjusting the spacing between PCBs. The effectiveness of natural convection cooling using air as the medium depends largely on two main factors; the heat flux dissipated by the chips and the spacing between adjacent PCBs. Since the heat flux is difficult to control, optimizing the spacing between PCBs is the most practical way. As shown in Figures 3.30 and 3.31, the maximum temperature can be lowered by increasing the spacing length for a given value of heat flux.

The results obtained indicate that at high enough Grashof number (about 3×10^5 for the first case and 2×10^5 for the second), the steady state laminar flow solutions become time-dependent. These results can be used in designing more elaborate cooling methods, for example, by combining natural convection with fan driven flow. Knowing the natural frequency of the spontaneously oscillatory free convection flows, forced convection can be applied to create resonance effects and consequently enhance the cooling rate.

The results for turbulent flow reported in this thesis are not as reliable as those for laminar flow, due to the uncertainties in the mixing length model. However, the author hopes that the results can be used as a basis for further studies in this area.

The isotherm and streamline contour plots presented here are in agreement with those reported by Liakopoulos et al. (1991) for tall enclosures with periodically spaced protruding heat sources. Therefore, the flow phenomena and heat transfer characteristics of the middle sections of tall cavities with protruding heat sources can be approximated by solving the equations for only one periodicity unit. This approximation greatly reduces the computational burden.

REFERENCES

Afrid, M., and Zebib, A., 1989, *Natural Convection Air Cooling of Heated Components Mounted on a Vertical Wall,* Numerical Heat Transfer, Part A, Vol 15, pp. 243-259.

Arsenault J. E. and Roberts, J. A., 1980, *Reliability and Maintainability of Electronic Systems*, Computer Science Press, pp. 162-191.

Canuto, C., Hussaini, M.Y., Quarteroni, A. and Zang, T.A., 1989, *Spectral Methods in Fluid Dynamics,* Springer, New York.

Cheung, F.B., and Sohn, D.Y., 1989, *Numerical Study of Turbulent Natural Convection in an Innovative Air Cooling System,* Numerical Heat Transfer, Part A, Vol. 16, pp. 467-487.

Chung, Jeilung, 1987, *Predicting Maximum Enclosure Temperature,* Machine Design, pp. 101-107.

Dally, James W., 1990, *Packaging of Electronic Systems*, McGraw-Hill, pp. 3-5.

Fischer, P.F., Ho, L.W., Karniadakis, G.E., Ronquist, E.M., and Patera, A. T., 1988, *Recent Advances in Parallel Spectral Element Simulation of Unsteady Incompressible Flows,* Computer and Structures, Vol. 30, No. 1/2, pp. 217-225.

Fuqua, Norman B., 1987, *Reliability Engineering for Electronic Design*, Marcel Decker, pp. 36-39, 229-241.

Huang, X. and Liakopoulos, A., 1991, *Spectralview: A Computer flow visualization and data analysis package,* Lehigh University.

Incropera, F.P., and De Witt, D.P., 1990, *Fundamentals of Heat and Mass Transfer*, John Wiley & Son, pp. 312-369, 529-570.

Kelleher, M.D., Knock, R.H., and Yang, K.T., 1987, *Laminar Natural Convection in a Rectangular Enclosure Due to a Heated Protrusion on One Vertical Wall Part I: Experimental Investigation,* Proceedings, 2nd

ASME/JSME Thermal Engineering Joint Conference, Honolulu, HI, Vol. 2, pp. 169-177.

Keyhani, M., Chen L., and Pitts, D.R., 1991, *The Aspect ratio Effect on Natural Convection in an Enclosure with Protruding Heat Sources*, Journal of Heat Transfer, Vol. 113, pp. 883-891.

Lee, J.J., Liu, V.K., Yang, K.T., and Kelleher, M.D., 1987, *Laminar Natural Convection in a Rectangular Enclosure Due to a Heated Protrusion on One Vertical wall Part II: Numerical Simulation,* Proceedings, 2nd ASME/JSME Thermal Engineering Joint Conference, Honolulu, HI, Vol. 2, pp. 179-185.

Liakopoulos, A. and Blythe, P.A. , Simpkins, P.G., 1990, *Convective Flows in Tall Cavities,* in Simulation and Numerical Methods in Heat Transfer, ASME, HTD-Vol. 157, pp. 81-87.

Liakopoulos, A., Huang, X., Blythe, P.A, and Simpkins, P. G., 1991, *Buoyancy Driven Motions Due to a Vertical Array of Heat Sources,* Heat Transfer in Electronic Equipment ASME, HTD-Vol. 171, pp. 63-69.

Miyamoto, M., Katoh, Y., Kurima, J., Sasaki, H., 1986, *Turbulent Free Convection Heat Transfer from Vertical Parallel Plates,* Proc. 8th International Heat Transfer Conference, Vol. 4, pp. 1593-1598.

NEKTON Users Manual, Relase 2.2, 1989, Nektonics Inc.

Patera, A. T., *1984, A Spectral element method for Fluid Dynamics: Laminar Flow in a Channel expansion,* J. Comp. Phys. 54, pp. 468-488.

Simon, Robert E. , 1983, *Thermal Management of Electronic Packages*, Solid State Technology, October, pp. 64-65

Yanenko, N. N., 1971, *The method of fractional steps for solving multi-dimensional problems of mathematical physics in several variables,* Springer.

Vita

Masdi Muhammad

The author was born in Kuala Krai, Kelantan, Malaysia on the 4th of August , 1968. The eldest son of Muhammad Ismail and Siti Rahimah Abd Ghani, his siblings are Masniza, Mazli, Marzuki and Mazwan. He and his wife, Lily, are blessed to have a wonderful son, Muhammad Kushairy, who was born in February 1991.

Masdi Muhammad received his B.S in Mechanical Engineering from Lehigh University in 1991. He is pursuing his M.S in Manufacturing Systems Engineering at the same university and expects to receive his degree in May 1992. He is currently a member of ASME, SME and is involved actively in the Lehigh University International Club.

The author has been working as a Research Assistant at Lehigh University since January 1991, in the field of heat transfer. He has recently accepted a position as an engineer in Research and Development with INTEL TECHNOLOGY in Malaysia.

END

OF

TITLE